Structural Design Elements in Biological Materials: Application to Bioinspiration

ARTICLE *in* ADVANCED MATERIALS · AUGUST 2015

Impact Factor: 17.49 · DOI: 10.1002/adma.201502403 · Source: PubMed

4 AUTHORS:

Steven E. Naleway
University of California, San Diego
15 PUBLICATIONS **24** CITATIONS
SEE PROFILE

Michael M Porter
Clemson University
44 PUBLICATIONS **72** CITATIONS
SEE PROFILE

Joanna Mckittrick
University of California, San Diego
198 PUBLICATIONS **2,834** CITATIONS
SEE PROFILE

Marc A Meyers
University of California, San Diego
484 PUBLICATIONS **11,198** CITATIONS
SEE PROFILE

Structural Design Elements in Biological Materials: Application to Bioinspiration

Steven E. Naleway, Michael M. Porter, Joanna McKittrick, and Marc A. Meyers**

Eight structural elements in biological materials are identified as the most common amongst a variety of animal taxa. These are proposed as a new paradigm in the field of biological materials science as they can serve as a toolbox for rationalizing the complex mechanical behavior of structural biological materials and for systematizing the development of bioinspired designs for structural applications. They are employed to improve the mechanical properties, namely strength, wear resistance, stiffness, flexibility, fracture toughness, and energy absorption of different biological materials for a variety of functions (e.g., body support, joint movement, impact protection, weight reduction). The structural elements identified are: fibrous, helical, gradient, layered, tubular, cellular, suture, and overlapping. For each of the structural design elements, critical design parameters are presented along with constitutive equations with a focus on mechanical properties. Additionally, example organisms from varying biological classes are presented for each case to display the wide variety of environments where each of these elements is present. Examples of current bioinspired materials are also introduced for each element.

1. Introduction

In spite of an estimated 7 million animal species living on earth,[1] there is remarkable repetition in the structures observed among the diversity of biological materials. This is due to the fact that many different organisms have developed similar solutions to natural challenges (e.g., ambient environmental conditions, predation). As a result, the vast body of research on biological materials often presents similar solutions, since the number of materials available in nature is fairly limited and therefore resourceful combinations of them have to be developed to address specific environmental constraints. We have identified these common designs and named them "structural design elements."

In the emerging field of biological materials science, there is a great need for systematizing these observations and to describe the underlying mechanics principles in a unified manner. This is necessary as similar designs are often reported under various names. As an example, the presence of numerous interfaces within a composite that introduce a significant property mismatch, which we suggest be named a "layered" structure, has been previously referred to as "lamella" in bone[2] and fish scales,[3] "brick and mortar" in abalone,[4–6] and a "laminated structure" in sea sponges[7] despite providing most if not all of the same structural advantages. We propose herein a new system of eight structural design elements that are most common amongst a wide variety of animal taxa. These structural elements have each evolved to improve the mechanical properties, namely strength, stiffness, flexibility, fracture toughness, wear resistance, and energy absorption of different biological materials for specific multi-functions (e.g., body support, joint movement, impact protection, mobility, weight reduction). These structural design elements are visually displayed in **Figure 1**:

- **Fibrous** structures; offering high tensile strength when aligned in a single direction, with limited to nil compressive strength.
- **Helical** structures; common to fibrous or composite materials, offering toughness in multiple directions and in-plane isotropy.
- **Gradient** structures; materials and interfaces that accommodate property mismatch (e.g., elastic modulus) through a gradual transition in order to avoid interfacial mismatch stress buildup, resulting in an increased toughness.
- **Layered** structures; complex composites that increase the toughness of (most commonly) brittle materials through the introduction of interfaces.
- **Tubular** structures; organized porosity that allows for energy absorption and crack deflection.
- **Cellular** structures; lightweight porous or foam architectures that provide directed stress distribution and energy absorption.

S. E. Naleway, Prof. J. McKittrick, Prof. M. A. Meyers
Materials Science and Engineering Program
University of California
San Diego, La Jolla, CA 92093–0411, USA
E-mail: snaleway@eng.ucsd.edu;
mameyers@eng.ucsd.edu
Prof. M. M. Porter
Department of Mechanical Engineering
Clemson University
Clemson, SC 29634, USA
Prof. J. McKittrick, Prof. M. A. Meyers
Department of Mechanical and Aerospace Engineering
University of California
San Diego, La Jolla, CA 92093–0411, USA
Prof. M. A. Meyers
Department of Nanoengineering
University of California
San Diego, La Jolla, CA 92093–0411, USA

DOI: 10.1002/adma.201502403

These are often surrounded by dense layers to form sandwich structures.
- **Suture** structures; interfaces comprising wavy and interdigitating patterns that control strength and flexibility.
- **Overlapping** structures; featuring multiple plates or scutes that overlap to form flexible and often armored surfaces.

As with all biological materials, these structural design elements are composed of biopolymers (e.g., collagen, chitin, keratin) and biominerals (e.g., calcium carbonate, calcium phosphates, silica) that are hierarchically assembled from the nano- to mesoscales.[8–10] However, the extraordinary mechanical properties observed in these natural materials are often a product of the intricate structural organization at different spatial scales (nano, micro, meso, and macro) where these structural design elements are observed (**Table 1**). As a result, in many cases organisms with different base materials will employ the same structure for the same purpose (e.g., tubules found in human dentin composed of hydroxyapatite/collagen and also in ram horns composed of keratin[11] can both absorb energy).

Examples of the structure–function relationships of the common structural design elements in biological materials can be found in a number of different organisms from varying biological classes (shown herein), illustrating the wide range of environments where these design elements are observed. In addition, bioinspired materials that incorporate these common structures are becoming more prevalent as modern manufacturing allows for more control at the important spatial scales where these design elements are most often present. This paper organizes these eight elements by their relative size and complexity (e.g., from smaller, less-complex fibrous structures to larger, more-complex overlapping structures) and provides constitutive equations that describe their basic mechanical and/or structural advantages.

2. Fibrous Structures

Biological materials that require high tensile strength or stiffness in a single direction are organized as fibrous structures, designed with numerous aligned fibers (and fibrils or filaments at smaller spatial scales) that often exhibit hierarchy across multiple length scales (**Figure 2**a). They are commonly found within non-mineralized, soft biological materials, such as muscle, tendon, and silks. However, there are a number of notable exceptions such as the chitin fibers in arthropod exoskeletons and collagen fibers in bones where these fibers are mineralized. These structures occur within the nano- to microstructures of biological materials. Specific examples given here are spider silk (Figure 2b),[14,33] hagfish slime (Figure 2c),[12,34,35] silkworm silk (Figure 2d)[8] and rat tendon (Figure 2e).[13,36]

Mechanically, fibrous structures present a dichotomy of strength, high in tension and low to effectively nil in compression. This results in dramatic tension–compression asymmetric behavior. Thus, they are typically applied in a tensile mode and are only described as such here. These materials tend to exhibit a characteristic *J*-shaped stress–stain curve resulting in two regimes of elastic-plastic behavior. In the first of these regimes the aligned fibers unfurl, slide past each other, and straighten without significant resistance, following the power law (Figure 2f(i) to 2f(ii)).[41]

$$\frac{d\sigma}{d\varepsilon} \propto \varepsilon^n (n > 1) \quad (1)$$

where σ is the stress, ε is the strain, and n varies with the material, with $n = 1$ associating with the mechanical behavior of aligned collagen.[42] A number of models have been presented in order to characterize the unfurling and straightening of the

Steven E. Naleway is a Ph.D. candidate in the Materials Science and Engineering Program at the University of California, San Diego. He received his B.S. degree in Mechanical Engineering and M.S. degree in Materials Science both from Oregon State University. His research focuses upon the interconnected fields of biological materials science and bioinspired design both with a focus upon structural applications.

Joanna McKittrick has a B.S. in Mechanical Engineering from the University of Colorado, a M.S. in Materials Science and Engineering from Northwestern University and a Ph.D. in Materials Science and Engineering from MIT. She works in the area of the structure-mechanical properties (strength, stiffness, toughness, impact resistance) of biological composites and developing bioinspired designs. She also works in the area of luminescent materials, most recently on phosphor development for solid-state lighting.

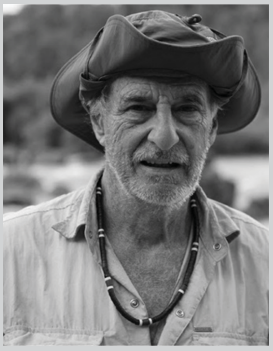

Marc André Meyers is a distinguished professor at the University of California, San Diego. He focuses his research on the mechanical behavior of materials. He is a Fellow of TMS, APS, and ASM and a member of the Brazilian Academy of Sciences.

DOI: 10.1002/adma.201502403

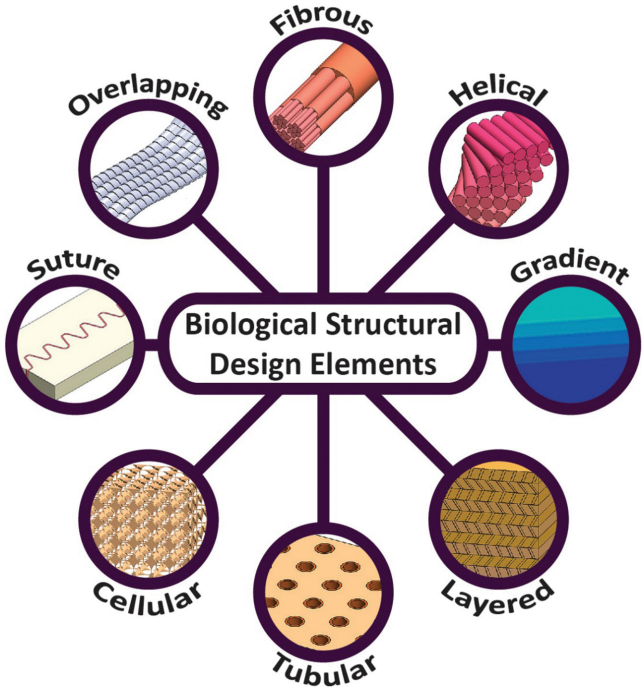

Figure 1. Diagram of the eight most common biological structural design elements.

fibers during this initial regime. These include modeling the waviness as a sine function,[43] a helical structure,[44] or as circular segments.[45] Additionally, the initial mechanical behavior, as the fibers first begin to slide past one another, has been modeled as a dashpot–spring series combination to account for viscoelasticity.[45] In the second regime, the fibers become taut and experience increased strain, resulting in a higher and effectively linear stiffness following Hooke's law, adapted from ref.[41] (Figure 2f(iv)):

$$\frac{d\sigma}{d\varepsilon} = E \tag{2}$$

where E is the elastic modulus. To form a single constitutive equation, Equation (1) and Equation (2) can be integrated and combined to form Equation (3), describing the comprehensive stress–strain behavior of fibrous structures in tension:[41]

$$\sigma = k_1\varepsilon^{n+1} + H(\varepsilon_c)E(\varepsilon - \varepsilon_c) \tag{3}$$

where k_1 is a material parameter and H is the Heaviside function, which activates when the second regime is reached ($\varepsilon = \varepsilon_c$, where ε_c is the characteristic strain at which the fibers have become fully extended). This simplified equation by Meyers et al.[41] can be replaced by more complex constitutive equations originally derived for polymers by Ogden[46] and Arruda and Boyce,[47] and specifically applied to biological tissue by Fung.[48]

As a result of the physical unfurling of fibers associated with the first regime of elastic–plastic behavior, the initial ordering of a fibrous structure (e.g., wave/kink of the individual fibers, interweave of fibers, length of fibers, sliding between fibrils) determines a broad range of mechanical responses that are often tailored to specific needs. This *J*-curve elastic–plastic behavior is critical for many biological materials. Specifically, the nature of these materials, where the rate of change of the slope increases with strain, initially allows for a large amount of deformation with minimal energy consumption followed by a large energy consumption before fracture. In tendons and muscles, this allows for energy savings on small tasks while maintaining high stiffness needed for heavy lifting. In the silk of spider webs, at low stress the web is flexible, allowing the spider to detect the small vibrations of trapped prey. However, the same web is much stiffer at high stress to avoid fractures that could allow prey to escape.

3. Helical Structures

Helical structures generally provide increased strength and toughness in multiple directions by employing numerous fibers, fibrils, or reinforcements at varying angles (**Figure 3**a). These structures are often employed in non-mineralized or relatively low-mineralized structural materials, which can be referred to as twisted-ply structures. Though often formed from the same constituents as fibrous structures, helically organized fibrous structures can result in in-plane isotropy and enhance the toughness of the resulting material. When formed in the macrostructure, helically reinforcing structures are most often employed on exterior surfaces to improve the torsional rigidity. Twisted-ply structures occur in the nano- to microstructures while helically reinforcing structures generally occur in the macrostructure of biological materials and organisms. Specific examples include crustacean exoskeletons (e.g., stomatopod dactyl club, Figure 3b)[16] and mammalian bone collagen (e.g., rat, Figure 3c),[49] highly mineralized sea-sponge exoskeletons (Figure 3d),[7,50] insect exoskeletons (e.g., grasshopper, Figure 3e)[15,51] and fish scales.[31,52,53] In the idealized arrangement described by Bouligand,[51] each layer of fibers is rotated from the previous stacked layer by a constant angle and the arrangement completes a full 180° rotation. However, many variations of this structure have been observed in biological materials with rotations at varying angles or even in opposing directions, where these arrangements can provide significant resistance to mechanical stress (e.g., the increased puncture resistance in orthogonally aligned fish scales).[52,54,55]

Mechanically, less-mineralized helical structures provide three principal structural attributes: i) they provide increased isotropy in multiple directions along the fiber plane by stacking layers of fibers or fibrils at varying angles (**Figure 4**a), ii) they provide increased toughness as the misaligned fiber planes can distract crack advance, forcing it to propagate in multiple planes (Figure 4b), and iii) the aforementioned isotropy provides a significant increase in the compressive strength and stiffness over fibrous structures, despite consisting of the same constituents. Perhaps most impressive is that many twisted-ply structures are capable of realigning their fibrous structure to accommodate external forces applied in-plane (as shown schematically in Figure 3f).[52,53]

Table 1. Length scales of each structural design element along with representative examples. In each case, dimensions are given that represent the characteristic length scale (i.e., fiber diameter, helical layer/reinforcement thickness, gradient thickness, layer thickness, tubule diameter, cell diameter, suture wavelength, overlapping plate length). These dimensions are meant to provide an understanding of the length scales at which these structures occur, as dimensions vary with species.

Fibrous		
Nano- to microscale		
Hagfish slime intermediate *k* Filaments: 10 nm[12]	Collagen fibril: 100–500 nm[13]	Spider silk: <10 μm[14]
Helical		
Nano- to microscale (twisted-ply) or macroscale (reinforcement)		
Beetle exoskeleton: 50–200 nm[15]	Stomatopod club: ca. 75 μm[16]	Sea sponge ridge: ca. 1 mm[7]
Gradient		
Micro- to macroscale		
Tooth dental/enamel junction: ca. 20 μm[17]	Crab claw: 10–20 μm[18]	Squid beak: ca. 50 mm[19]
Layered		
Microscale		
Sea sponge spicule: 0.2–1.5 μm[7]	Abalone nacre: ca. 0.4 μm[4]	Fish scale: ca. 25–50 μm[20]
Tubular		
Microscale		
Tooth dentin: ca. 1 μm[21]	Fish scale: ca. 6.5 μm[22]	Horn tubule: ca. 40–100 μm[23]
Cellular		
Nano- to microscale (sandwich) or macroscale (bulk)		
Porcupine quill: ca. 100 nm[24]	Elk antler: ca. 300 μm[25]	Coral: 10–40 μm[26]
Suture		
Microscale		
Boxfish scute: ca. 65 μm[27]	Turtle shell: 230–400 μm[28]	Deer skull: 640–2500 μm[29]
Overlapping		
Macroscale		
Seahorse plate: 1–10 mm[30]	Striped bass scale: 8–10 mm[31]	Chiton plate: ca. 5 mm[32]

As there is a current lack of constitutive equations describing the mechanics of helical structures, we provide our own interpretation. Such an in-plane isotropy is accomplished by the layering of highly anisotropic fibers along different orientations. Figure 4a displays the proposed arrangement where fibers are subjected to an external load or tension, T. Note that, in this example all of the fibers make discrete and equal angles, α, to each other and rotate a full 180° thus creating a Bouligand structure. However, the same could be applied for a structure consisting of varying angles (e.g., α_1, α_2, α_3). In this model, we assume that the fiber(s) perfectly aligned with the direction of tension are fully loaded. In other fibers, we assume that the tensile load decreases with the cosine of the angle:

$$T = F_0 + F_\alpha \cos(\alpha) + F_{2\alpha} \cos(2\alpha) + \cdots + F_{-\alpha} \cos(-\alpha) + F_{-2\alpha} \cos(-2\alpha) + \cdots \quad (4)$$

where F_0 is the force experienced by fibers oriented parallel to the loading direction and $F_{i\alpha}$ is the load resisted by each individual fiber. In the case of tensile loading, those fibers are only capable of resisting load in the direction of tension. Therefore, Equation (4) can be modified in order to account only for the force resisted in the loading direction:

$$T = F_0 + F_0 \cos^2(\alpha) + F_0 \cos^2(2\alpha) + \cdots + F_0 \cos^2(-\alpha) + F_0 \cos^2(-2\alpha) + \cdots \quad (5)$$

which can also be simplified to a summation:

$$T = F_0 \sum_{i=1}^{n} \left[1 + 2\cos^2(i\alpha)\right] \quad (6)$$

This relationship holds for any loading orientation within the fiber plane, thus creating an effective in-plane isotropy. This force can be converted to stress by dividing it by the combined projected area, normal to the direction of loading, of all the fibers.

The relatively high toughness of helical structures is the result of an increase in resistance to crack propagation due to the differing orientations of the fiber layers. Figure 4b displays an example four-layer helical structure where the angle between the layers is roughly 45°. Each layer reacts differently to a propagating crack tip (Figure 4b(i) to 4b(iv)). Layers parallel (Figure 4b(iii)) to the crack growth front undergo separation, while those at an angle (Figure 4b(ii) and 4b(iv)) deflect the crack and layers perpendicular (Figure 4b(i)) provide significant resistance as the fibers will need to fracture before the crack can propagate. Thus fracture, separation, and deflection, along with the previously mentioned rotation of fibers, all contribute to the delocalization of the stresses at the crack tip. Dastjerdi and Barthelat[31] have experimentally demonstrated this effect in teleost fish scales, and shown that these mechanisms allow the scales to be amongst the toughest biological materials known. In addition, through studies on the stomatopod dactyl club, the periodicity of these helical structures has recently been shown to be capable of filtering shear waves induced during dynamic loading, thus increasing the impact resistance of the biological material.[57] The scattering effect on waves by multiple layers is an important energy-dissipation mechanism.

Another type of helical structure often observed in nature is that generally found in connection with continuous helices. These are usually found along the outer plane of cylindrical-like organisms (e.g., narwhal tusks[58] and glass sponges[50] (Figure 4d)) as well as many woody plants,[59] acting as a reinforcing structure to resist the bending and torsion caused by environmental stresses (e.g., ocean currents). Such external helical-reinforcements grow in response to induced torsion and provide a significant amount of

Adv. Mater. **2015**,
DOI: 10.1002/adma.201502403

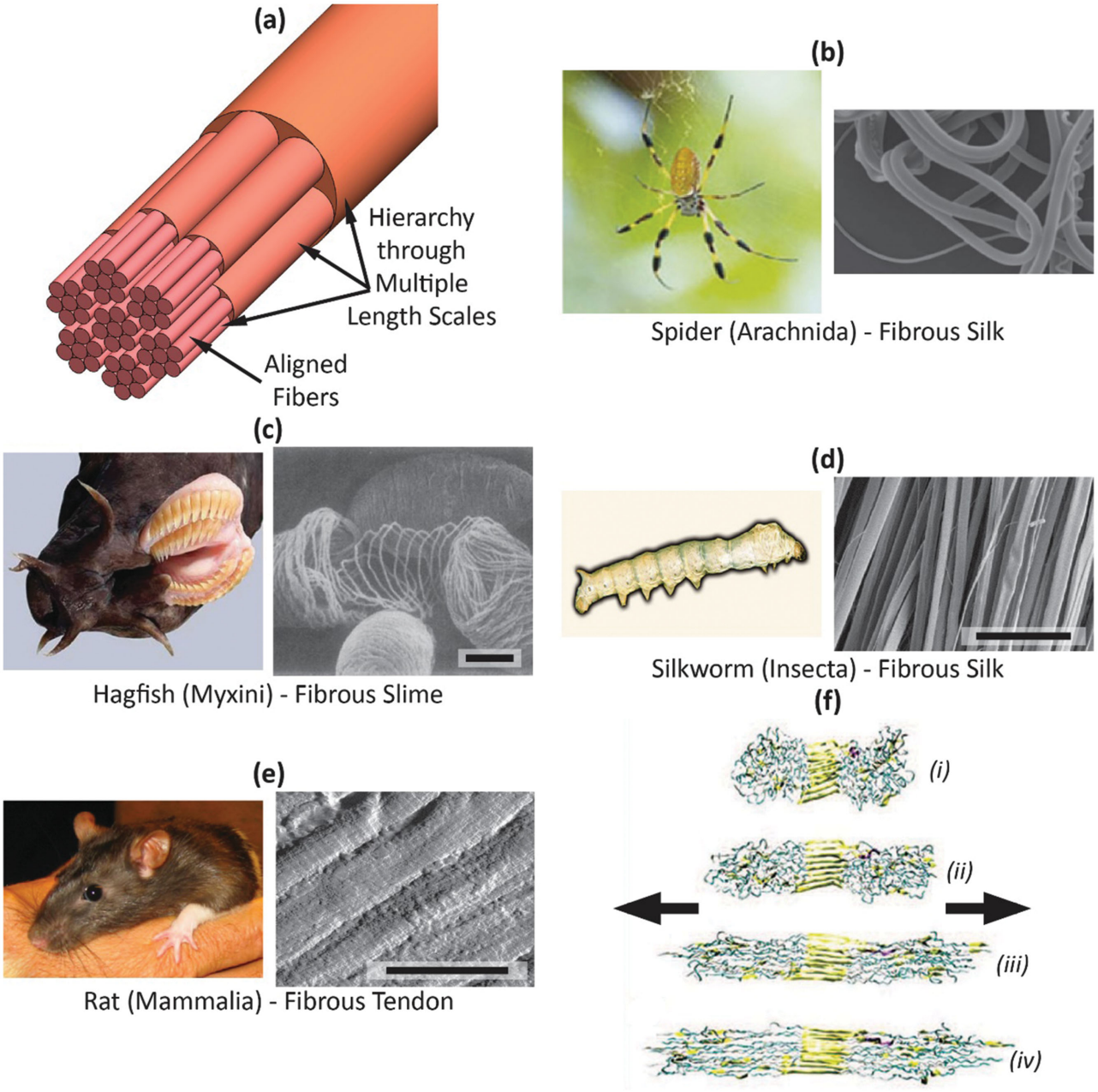

Figure 2. Biological fibrous structures from nature representing a variety of biological classes. a) Diagram of fibrous structures with a hierarchy of aligned fibers at multiple length scales; b) Spider (Arachnida) with fibrous silk; c) Hagfish (Myxini) with fibrous slime; d) Silkworm (Insecta) with fibrous silk; e) Rat (Mammalia) with fibrous tendons; f) Diagram of fibrous structures pulled in tension demonstrating how the fibers align then strain in unison. Scale bars: 20 μm (c), 100 μm (d), 100 μm (e). b) Adapted with permission.[37] Copyright 2009, John Wiley and Sons; c) Adapted with permission.[38] Copyright 2012, Springer (left) and adapted with permission.[39] Copyright 1981, The American Association for the Advancement of Science (right); d) Adapted with permission.[40] 2008, Elsevier (left) and adapted with permission[8] Copyright 2008, Elsevier (right); e) Adapted with permission.[9] 2012, Elsevier (left) and adapted with permission.[13] Copyright 2002, Elsevier (right); f) Adapted with permission.[41] 2013, The American Association for the Advancement of Science.

torsional rigidity along their cylindrical axes.[60] As seen in Figure 4d,[50] these reinforcing ridges typically grow ca. 45° to the cylindrical axis that, under an applied torque, is oriented parallel to the directions of maximum compressive and tensile stresses that build-up in these materials. Similar to fiber-reinforced composite panels with angled fiber orientations, it can be shown that helix-reinforcements aligned at $\phi = 45^{\circ}$ with respect to the cylindrical axis provide a maximum normalized shear modulus $\left(G_{XY}/G_{12}\right)$ in these types of structures:[60]

$$G_{XY}/G_{12} = \frac{1}{m^4 + n^4 + 2m^2n^2\left[2\frac{G_{12}}{E_1}(1+2\nu_{12}) + 2\frac{G_{12}}{E_2} - 1\right]} \quad (7)$$

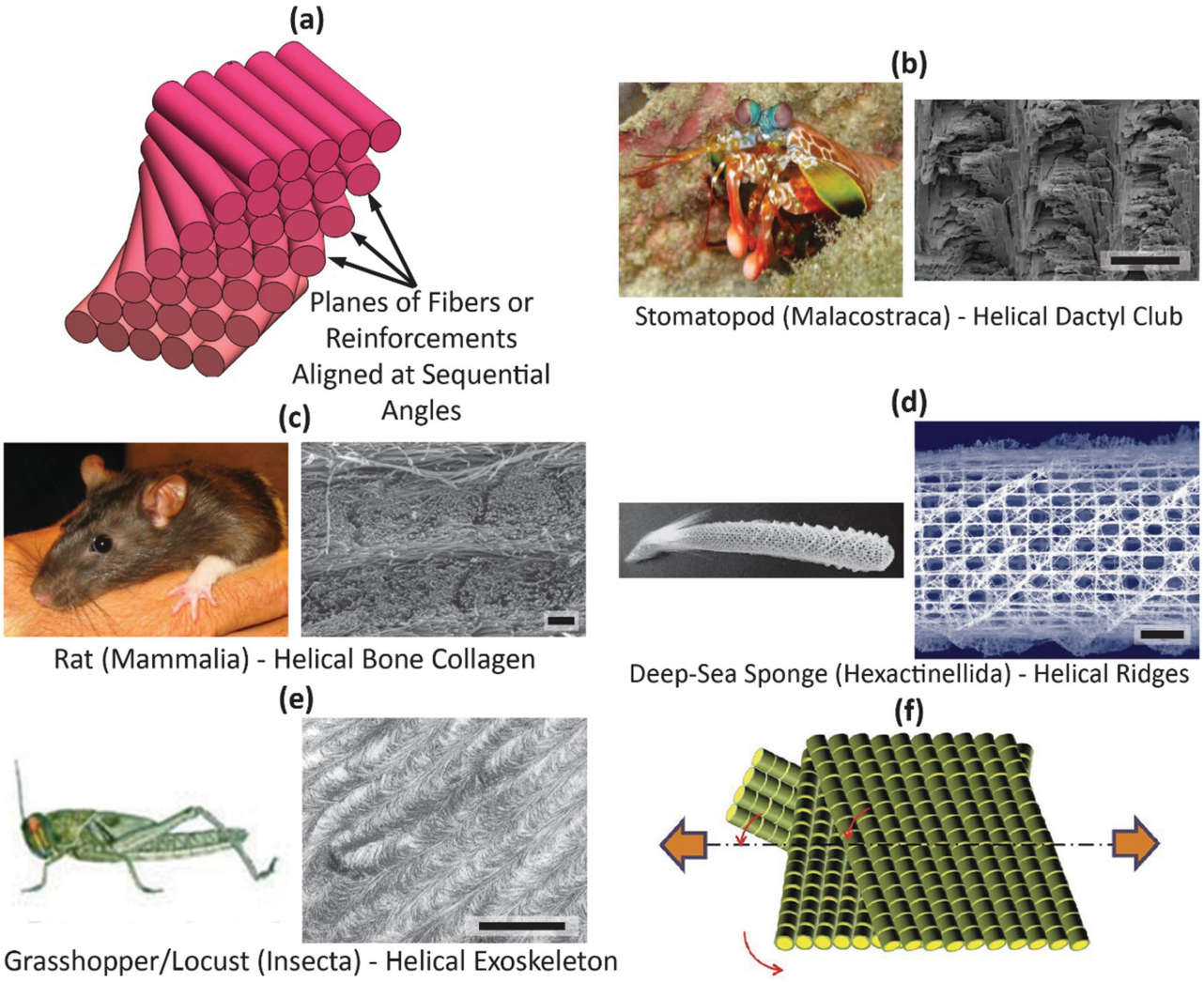

Figure 3. Biological helical structures from nature representing a variety of biological classes. a) Diagram of a helical structure showing planes of fibers or reinforcements aligned at sequential angles; b) Stomatopod (Malacostraca) with helical structures in its dactyl club; c) Rat (Mammalia) with helical collagen in its bones; d) Deep-sea sponge (Hexactinellida) with helical reinforcing ridges in its skeleton; e) Grasshopper/locust (Insecta) with helical structures in its exoskeleton; f) Diagram displaying how helical structures can rotate and align to better absorb tensile forces. Scale bars: 75 μm (b), 1 μm (c), 5 mm (d), 1 μm (e). b) Adapted with permission.[16] Copyright 2012, The American Association for the Advancement of Science; (c) Adapted with permission.[9] Copyright 2012, Elsevier (left) and adapted with permission.[49] Copyright 2012, Oxford University Press (right); d) Adapted with permission.[8] Copyright 2008, Elsevier; e) Adapted with permission.[56] Copyright 2010, Elsevier (left) and adapted with permission.[15] Copyright 2008, John Wiley and Sons (right); f) Adapted with permission.[52] Copyright 2013, Nature Publishing Group.

where $m = \cos\left(\frac{\pi}{2} - \phi\right)$ and $n = \sin\left(\frac{\pi}{2} - \phi\right)$, G_{XY} is the effective shear modulus of the material in the *XY*-plane (*X* is the circumferential axis and *Y* is parallel to the cylindrical axis), G_{12} and v_{12} are the shear modulus and Poisson's ratio in the 12-plane respectively (1 and 2 are axes parallel and perpendicular to the helix reinforcement), and E_1 and E_2 are the elastic moduli of the material parallel and perpendicular to the helical-reinforcement, respectively. Similar to these reinforcing helical structures, spirals are also found in the overall morphology of a wide variety of biological materials (e.g., antelope horns and seashells).[61,62] While spiral structures are ubiquitous in nature, the majority exists on a much larger size scale than the primary structural design elements discussed here. Therefore, we have omitted further discussion on spiral structures, which are detailed in original work by Thompson[61] and modeled by Harary and Tal.[62]

4. Gradient Structures

Gradient structures are composites that combine materials of varying mechanical properties or composition, resulting in a property or structure gradient through their cross-section or thickness, as opposed to an abrupt change (**Figure 5**a). These structural elements accommodate a property mismatch (e.g., elastic modulus, strength) between materials and provide toughness, resist wear, or arrest crack growth. They are commonly

Adv. Mater. **2015**,
DOI: 10.1002/adma.201502403

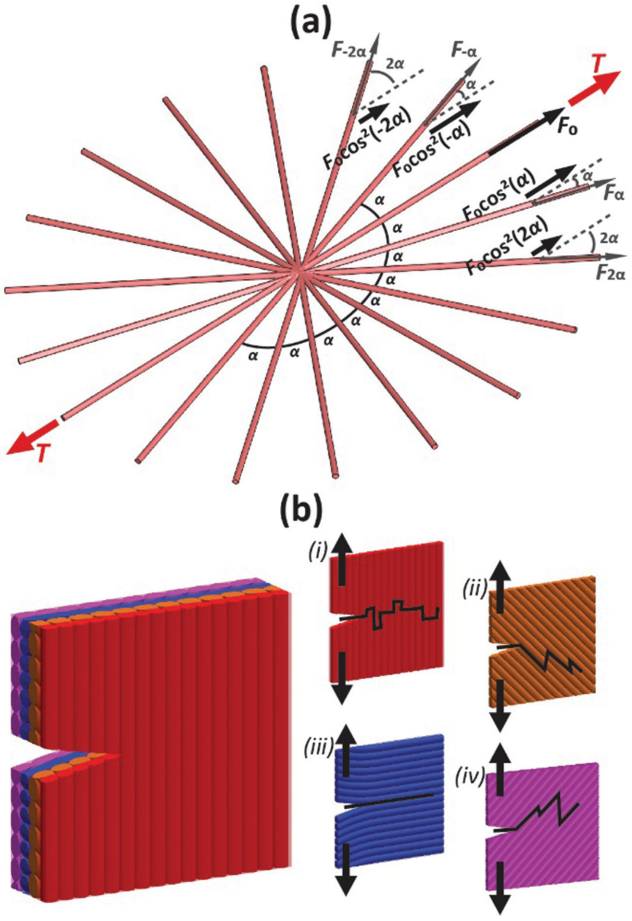

Figure 4. Examples of the mechanical advantages of helical structures. a) Fibers oriented in different directions allow for a load, T, applied in any direction to be resisted, thus creating in-plane isotropy. b) When a sharp crack grows within a helical structure, each offset plane results in a different preferred crack path (i)–(iv) thus increasing the fracture toughness.

found in dermal armors and teeth where rigid surfaces are combined with ductile bases. These gradient structures vary in size, from the microstructural dental/enamel junction (DEJ) in human teeth, which has been measured at ca. 20 μm (<1% of the total tooth thickness),[17] to the macrostructural squid beak where the gradient extends across the entire length.[19] Specific examples include gradients between the hard exterior and tough interior of fish scales (e.g., Senegal bichir, Figure 5b)[63] and crab claws (Figure 5c)[18] and the DEJ in many teeth (Figure 5d,e).[20,64]

Mechanically, gradient structures provide stress relief at the interfaces between dissimilar materials, which are characterized through a smooth transition in properties as is shown for the modulus through the thickness of a fish scale (Figure 5f).[20] Suresh,[65–67] Giannakopoulos,[68,69] Kim,[70,71] and co-authors have reported extensively on the mechanical and structural properties of gradient structures in many different loading configurations. Gradients can be described for a given mechanical property, Q, (e.g., elastic modulus, yield strength, toughness) as a function of position through the interface, z, adapted from ref.:[68]

$$Q = f(z) \quad \text{where: } f(z) = \begin{cases} \text{Linear}: Q_0(1-z) \\ \text{Power}: Q_0(1-z^k) \\ \text{Exponential}: Q_0 e^{-\alpha z} \end{cases} \tag{8}$$

where Q_0 is the initial value of the property (e.g., the value at the beginning or end of the gradient interface), k is a non-dimensional exponent that varies from $0 \le k < 1$ and α is a material constant with dimensions of length^{-1}. Equation (8) is presented so that, in each case, the value of Q begins at Q_0 then decreases throughout the gradient (for $\alpha >> 1$). While there are other possible profiles, the three listed here are those suggested and examined by Suresh and Giannakopoulos.[65,68] A gradient structure that follows a power-law relationship will become a linear gradient structure when $k = 1$ and a homogenous structure (non-gradient) when $k = 0$. For gradient structures that vary exponentially, $\alpha > 0$ results in a decrease through the bulk while $\alpha < 0$ inversely results in an increase through the bulk.

An abrupt or non-graded interface (similar to layered structures that will be discussed later) can impart additional toughness to a structure through interfacial crack deflection. However, gradient structures can serve to avoid interfacial stresses that exist between materials with significantly different mechanical (or thermal, optical, electromagnetic) properties. A prime example of this is the DEJ within mammalian teeth (Figure 5e). This well-bonded interface creates a gradient barrier between the stiff enamel and tough dentin phases. Importantly, this interface has been reported to arrest cracks propagating from the enamel to the dentin due to the elastic modulus mismatch.[17,72] An additional example, the squid beak, is a graded structure in which the hardness gradually decreases 100 times from the surface to the interior.[19,73]

5. Layered Structures

Layered structures are composite materials that consist of multiple layers or interfaces and are often employed to improve the toughness of otherwise brittle materials (**Figure 6**a). A foil to gradient structures, the interfaces in layered structures feature abrupt and often large changes in mechanical properties. Layered structures occur in the microstructure of biological materials. Specific examples include the concentric layers of deep-sea sponges (Figure 6b),[7,74] the brick and mortar structure of the abalone shell (Figure 6c),[4–6] the layers of many fish scales (e.g., the arapaima, Figure 6d)[20,53] and insect exoskeletons (e.g., beetles, Figure 6e).[15,75]

Mechanically, layered structures primarily increase the fracture toughness of a biological material through the introduction of numerous interfaces, which often contain a second more-ductile phase. Toughness is defined as the amount of energy a material can absorb prior to catastrophic failure. The fracture toughness is a measure of the energy required to induce catastrophic failure; however, it accurately assumes that inorganic materials contain flaws and cracks that reduce their strength from the theoretical value (ca. $E/10$ to $E/30$). With this assumption, the maximum stress before failure, σ_{max}, of any real material is governed by the Griffith equation:[77]

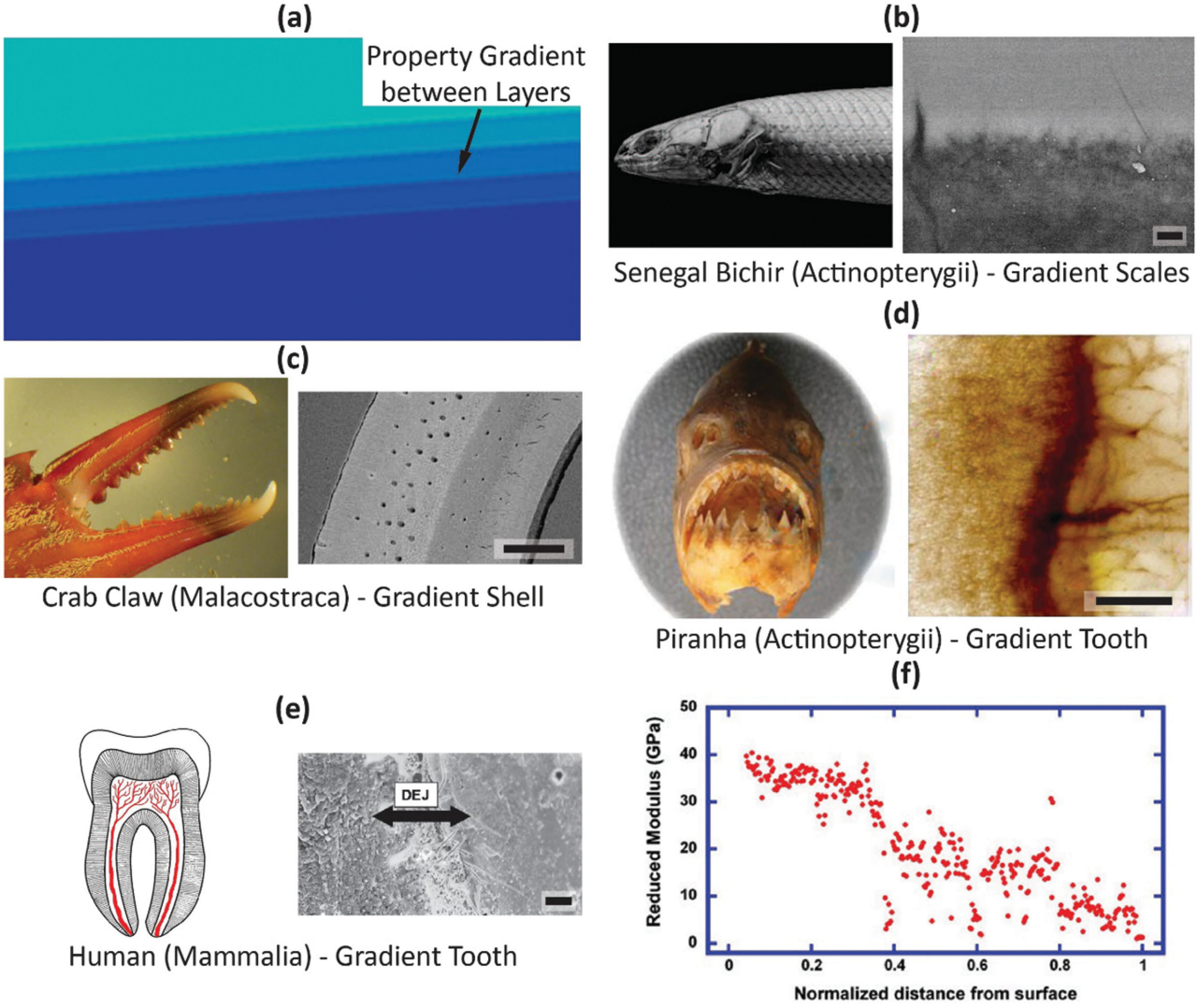

Figure 5. Biological gradient structures from nature representing a variety of biological classes. a) Diagram of gradient structures displaying a gradient in properties between layers; b) Senegal Bichir (Actinopterygii) with gradient scales; c) Crab (Malacostraca) with a gradient structure in its claws; d) Piranha (Actinopterygii) with a gradient dental-enamel junction (DEJ) in its teeth; e) Human tooth (Mammalia) with a gradient DEJ; f) Modulus data from a fish scale displaying the gradual shift in properties between layers through the scale thickness. Scale bars: 1 μm (b), 30 μm (c), 15 μm (d), 10 μm (e). b) Adapted with permission.[63] Copyright 2008, Nature Publishing Group; c) Adapted with permission.[18] Copyright 2009, Elsevier; d) Adapted with permission.[20] Copyright 2011, Cambridge University Press; e) Adapted with permission.[11] Copyright 2010, Elsevier (left) and adapted with permission.[64] Copyright 2008, Elsevier (right); f) Adapted with permission.[20] Copyright 2011, Cambridge University Press.

$$\sigma_{\max} = \sqrt{\frac{2\gamma E}{\pi a}} = \frac{YK_{Ic}}{\sqrt{\pi a}} \quad (9)$$

where γ is the material's energy that can be considered the sum of the surface energy (γ_s) and an energy related to plastic/permanent deformation ($\gamma = \gamma_s + \gamma_p$), a is the length of a crack or void in the material, Y is a geometric parameter, and K_{Ic} is the Mode I (opening) critical fracture toughness. This equation shows that the fracture strength and crack length are related by the material's parameter, K_{Ic}.

Unlike most helical structures that are generally found in more ductile materials, layered structures are most commonly composed of brittle constituents (e.g., calcium carbonate, hydroxyapatite, silica, and other biominerals), although they both impart toughness. Ritchie and co-workers[78–82] have reported extensively on the mechanisms that increase toughness in otherwise brittle materials. These mechanisms can be classified according to both their relative location with respect to a growing crack tip and their inherent length scale as either intrinsic (ahead of the crack tip, <1 μm) or extrinsic (behind the crack tip, >1 μm).[83] In layered biological structures, most toughening mechanisms are extrinsic, including crack deflection and twisting, uncracked ligament and fibril bridging, and microcracking. Each of these mechanisms serves to either increase the energy required to propagate a crack or shield stress from the crack tip. Among these, the energy required to cause catastrophic failure in most layered brittle biological materials is predominantly increased by

Adv. Mater. 2015,
DOI: 10.1002/adma.201502403

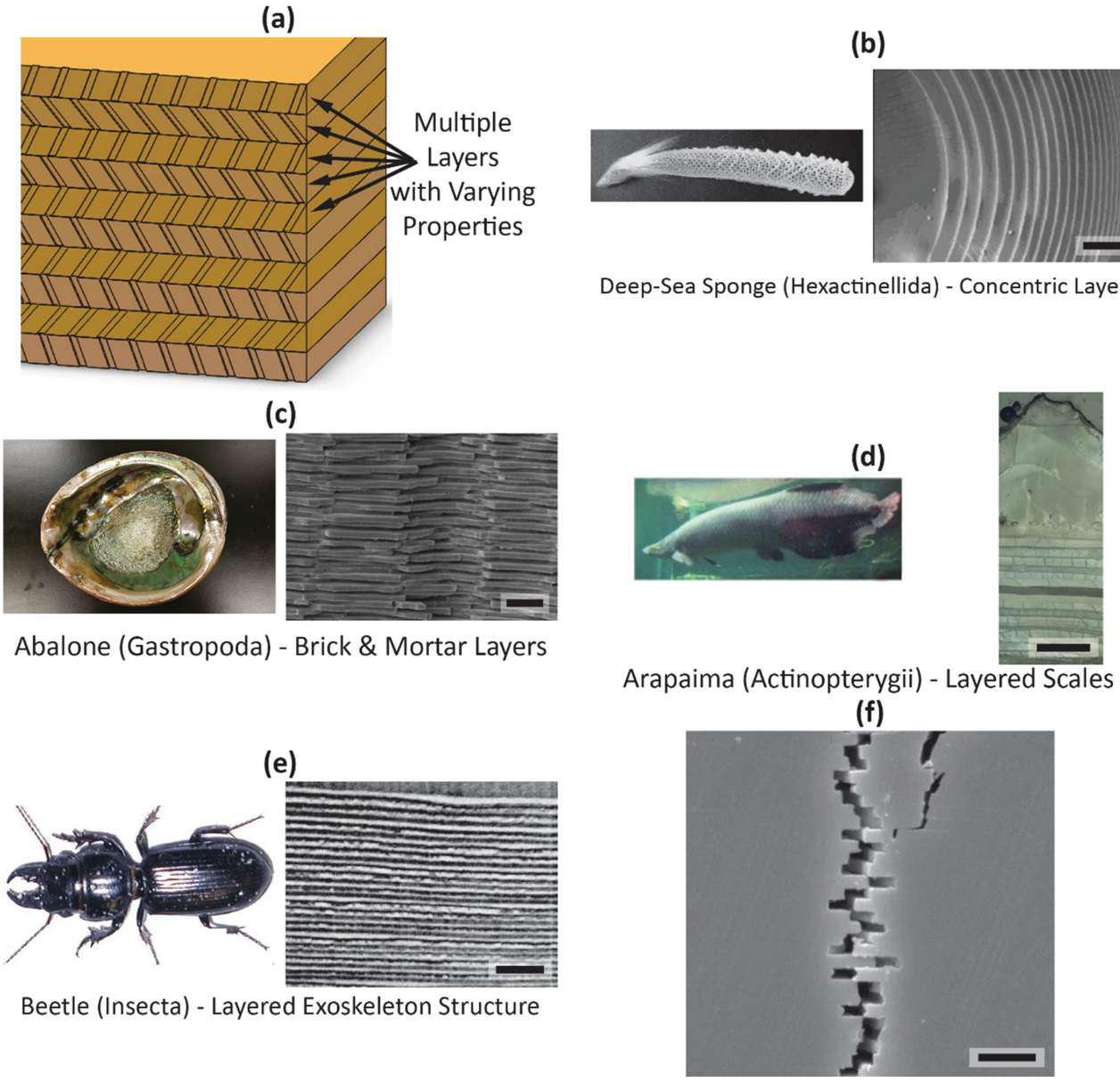

Figure 6. Biological layered structures from nature representing a variety of biological classes. a) Diagram of layered structures displaying multiple layers with varying properties or interfaces in order to induce anisotropy within the bulk material; b) Deep-sea sponge spicules (Hexactinellida) with concentric layers; c) Abalone shell (Gastropoda) with brick-and-mortar layers; d) Arapaima (Actinopterygii) with a layered structure through the cross-section of its scales; e) Beetle (Insecta) with a layered structure in its exoskeleton; f) Fracture image of a layered structure displaying how the layers deflect the crack and create a high energy, tortuous crack path. Scale bars: 5 μm (b), 2 μm (c), 200 μm (d), 1 μm (e), 2 μm (f). b) Adapted with permission.[8] Copyright 2008, Elsevier; c) Adapted with permission.[4] Copyright 2007, Elsevier; d) Adapted with permission.[9] Copyright 2012, Elsevier (left) and adapted with permission.[20] Copyright 2011, Cambridge University Press (right); e) Adapted with permission.[9] Copyright 2012, Elsevier (left) and adapted with permission.[15] Copyright 2008, John Wiley and Sons (right); f) Adapted with permission.[76] Copyright 2006, Elsevier.

two extrinsic mechanisms. First, by deflecting or twisting a crack, the applied stress is taken out of the preferred Mode I (opening) orientation, resulting in a more-tortuous crack path. Second, any deflection of the crack will result in an inherently longer crack path over a straight crack (as seen in Figure 6f), thus increasing the work required to propagate a crack, W_s:[77]

$$W_s = 2aB\gamma \tag{10}$$

where B is the out-of-plane thickness of the solid material. Though simplified, this provides an indication of the increase in toughness caused by the longer crack paths induced by predominately brittle layered structures. In addition to the increase in the cracked surface area, the introduction of relatively weaker interfaces can improve the toughness. As a crack approaches a weak interface, the stresses ahead of the crack tip can be sufficiently large to cause the interface to fracture. This creates, directly ahead of the crack tip, a second offset (or

ideally perpendicular) crack that, when merged, will significantly increase the crack-tip radius of curvature, ρ. This, known as the Cook–Gordon toughening mechanism, decreases the stress at the crack tip, σ_{tip}, as it is inversely related to ρ through the Inglis equation:[9]

$$\sigma_{tip} = \sigma_a \left(1 + 2\sqrt{\frac{a}{\rho}} \right) \quad (11)$$

where σ_a is the applied stress. It is this Cook–Gordon mechanism that is most effectively able to harness the numerous interfaces of layered structures in order to increase the facture toughness. However, the frictional sliding at the interfaces between lamellae created by crack deflection also contributes to the toughening in a manner similar to the toughening of fiber-reinforced composites. As a result, the toughness of many layered structures is much higher than a simple mixture of their constituents. The fracture toughness of abalone and conch, both of which have elements of a layered brick-and-mortar architecture (Figure 6c), is up to seven times higher than their main constituent, calcium carbonate, which makes up ca. 95% of their mass.[5,84]

6. Tubular Structures

Tubular structures consist of arrays of long aligned pores (tubules) within a bulk material (**Figure 7**a). These structural elements are commonly found in impact- and pierce-resistant materials, such as hooves, teeth, and the scales of fish. Tubules are microstructural elements in biological materials.

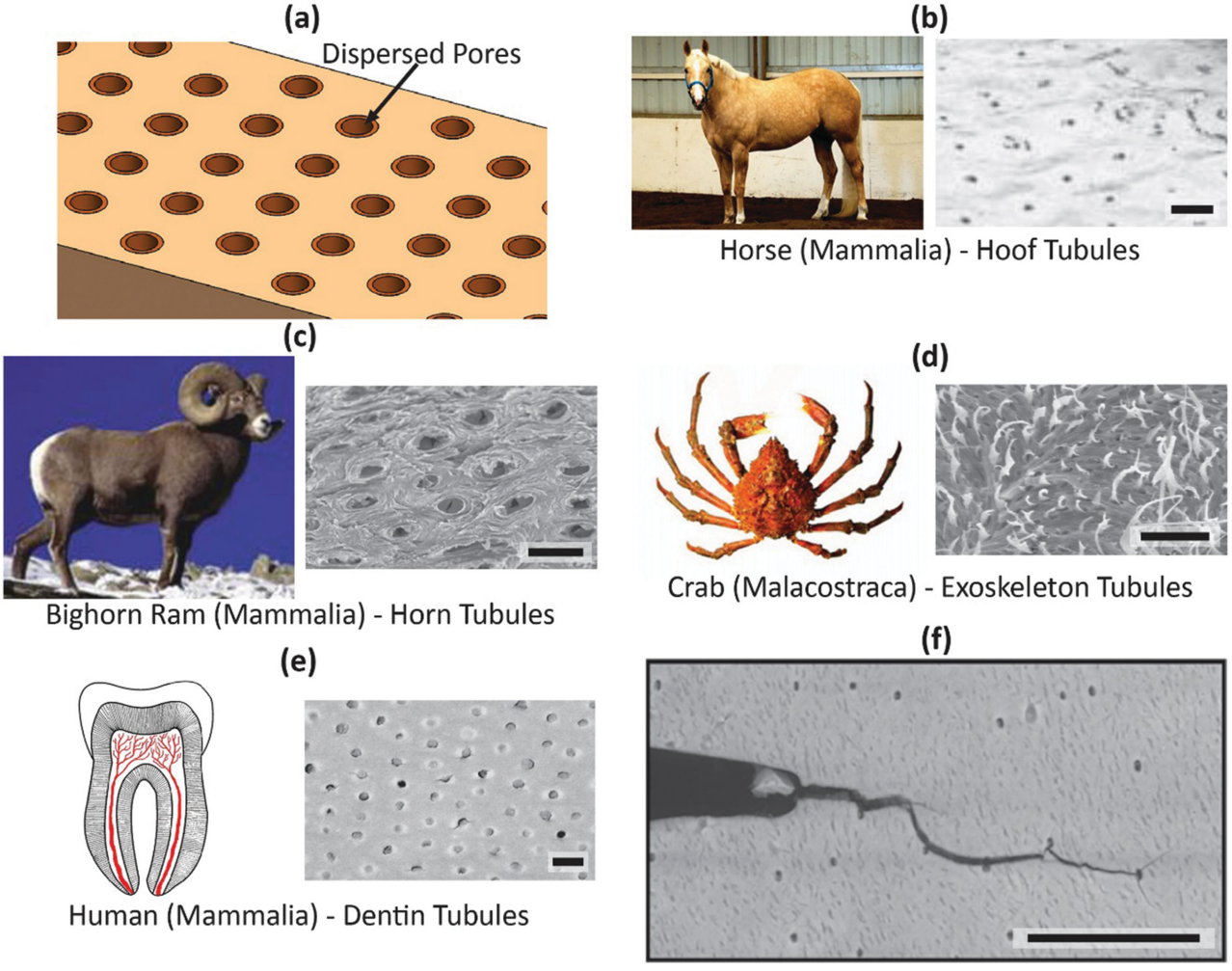

Figure 7. Biological tubular structures from nature representing a variety of biological classes. a) Diagram of dispersed tubules (pores) within a solid matrix; b) Horse (Mammalia) with hoof tubules; c) Bighorn ram (Mammalia) with horn tubules; d) Crab (Malacostraca) with exoskeleton tubules; e) Human tooth (Mammalia) with dentin tubules; f) SEM image of a material with tubules demonstrating how the tubules themselves can deflect a growing crack. Scale bars: 200 μm (b), 200 μm (c), 5 μm (d), 5 μm (e), 100 μm (f). b) Graciously donated by K. C. Fickas (left) and adapted with permission.[11] Copyright 2010, Elsevier (right); c) Adapted with permission.[88] Copyright 2003, Nature Publishing Group (left) and adapted with permission.[11] Copyright 2010, Elsevier (right); d) Adapted with permission.[87] Copyright 2008, Elsevier; e) Adapted with permission.[11] Copyright 2010, Elsevier; f) Adapted with permission.[22] Copyright 2013, Elsevier.

Adv. Mater. **2015**,
DOI: 10.1002/adma.201502403

Specific examples of materials that feature tubules include keratin-based horse hooves (Figure 7b)[85] and ram horns (Figure 7c),[23,86] chiton-based crab exoskeletons (Figure 7d),[87] collagen/hydroxyapatite-based human teeth (Figure 7e),[11] compact bone, and some fish scales.[22] Functionally, tubules provide nutrients (as is the case of dentin, osteons in bone and crustacean exoskeletons); provide ductile attachment (in crustaceans), and arrest cracks (in hooves, horns, fish scales). Mechanically, these structures improve fracture toughness and energy absorption by arresting crack growth through removing the stress singularity at the crack tip (Figure 7f) and/or by collapsing the tubules when compressed. They can also serve as scattering centers that decrease the amplitude of longitudinal stress pulses generated by impact. This is important in hooves and horns, which are subjected to high velocity loading (up to 10 m s^{-1}). This loading generates elastic waves of significant amplitude. The scattering of these waves can result in a decrease of their overall amplitude, thereby minimizing damage to the underlying live tissues.

Tubular structures that absorb energy through compression can be subdivided into those where the tubules are aligned perpendicular to the direction of loading (e.g., ram horn, Figure 7c)[23,86] and those where the tubules are aligned parallel to the direction of loading (e.g., horse hooves, Figure 7b).[85]

Tubular structures, which decrease the stiffness of structures but absorb energy during compression, can, mechanically, be modeled as hollow cylinders. Observing these structures in comparison to solid cylinders allows for the specific influence of the tubules to be assessed. Compression of an array of hollow cylinders (tubules) perpendicular to the long axis of the tubules results in a decrease in Young's modulus proportional to the volume fraction of the pores, adapted from ref.:[89]

$$\frac{E}{E_o} = \left(1 - V_p^2\right) \tag{12}$$

where E and E_o are the elastic moduli of the porous and dense material respectively and V_p is the volume fraction of the pores. Thus, the ratio of the displacement of a solid cylinder to a hollow cylinder is proportional to $\left(1 - V_p^2\right)$,[90] demonstrating that a much higher deformation can be achieved by incorporating aligned porosity than without it. Additionally, the relative elastic modulus (E/E_0) in the direction parallel to the tubules is also reduced (by a factor of $(1 - V_p)$), yielding a more-compliant structure than a solid material. Both of these effects result in the ability of the material to deform around the tubules, thereby increasing the energy absorbed over that of a material without tubules, for a constant applied force.

An example of a tubular structure that can absorb energy through compression is that in a sheep horn (Figure 7c). Sheep horns must be structurally robust as they undergo impact forces during seasonal fighting. Since they are a lifetime appendage, it is important that they do not fracture. Horns are composed of α-keratin and have a lamellar structure, which is stacked in the radial direction of the horn (parallel to growth direction), perpendicular to the direction of loading.[23] The lamellae are ca. 4 μm thick and have long tubules (ca. 40–100 μm in diameter) dispersed between the lamellae, and extending along the length of the horn, resulting in a porosity of ca. 7%. In spite of this small overall tubule density, the lamellar structure coupled with the tubules yields a material that can withstand large compressive stresses without fracture. Under compression in the radial (impact) direction, the tubules collapse allowing for 60% strain to be sustained without fracture.[23]

Similarly, the tubules of horse hooves (Figure 7b) are designed to absorb energy through compression. However, as opposed to horn, the tubular porosity is aligned parallel to the impact direction. The hoof wall has a complex structure consisting of tubular lamellae ranging from 6–15 μm in thickness. Hollow tubules (ca. 50 μm in diameter) are embedded in an intertubular matrix.[85] The tubular lamellae have a higher elastic modulus than the intertubular matrix, suggesting that the tubule structure, although porous, increases the elastic modulus of the hoof. In addition, Kasapi and Gosline[85,91] concluded that the tubules serve to increase crack deflection, thereby increasing the fracture toughness.

Mechanically, with the tubule orientation parallel to the direction of compressive loading, the compressive strength, σ_c, can be determined:[92]

$$\sigma_c = \frac{E_m\left(1 - V_p^{1/3}\right)\varepsilon_{mf}}{\nu_m} \tag{13}$$

where E_m is the elastic modulus of the matrix, ε_{mf} is the intertubular matrix strain at failure and ν_m is the Poisson's ratio of the matrix. From this, it can be seen that, because the tubules are reinforced, the compressive strength depends mainly on the strain to failure and elastic properties of the surrounding matrix.

The tubules in dentin (ca. 1 μm diameter) are well known to improve toughness and radiate from the pulp to the enamel surface, where there is a density of 3×10^4 mm^{-2} and, in addition to their mechanical advantage, allow for cellular activity and nutrient transport. The tubules are filled with a fluid and have a higher density of minerals surrounding them than the intertubular matrix. Therefore, dentin has often been modeled as a continuous fiber-reinforced matrix, with the highly mineralized tubules serving as the reinforcing fibers and the less-mineralized intertubular matrix as the surrounding phase.[21] Under normal compressive loading, the reinforced tubules are parallel to the load direction, similar to the hoof. The fracture toughness of dentin was found to be over 50% larger in the direction parallel to the tubules compared to the perpendicular direction, which was attributed to extensive crack bridging.[93]

In the freshwater Alligator gar fish scales, the tubules (6.5 μm diameter) with a density of ca. 300 mm^{-2} are oriented perpendicular to the surface of the scale.[22] The toughness and compressive strength is highest for loading parallel to the tubule direction compared to the two orthogonal directions, which is the optimal arrangement for resisting piercing attacks from biting predators. Similar to dentin, crack bridging was reported as the main factor in crack-growth resistance.

Tubules are present in the body of crustaceans, such as lobsters and crabs, and penetrate through the thickness of the exoskeleton (exo- and endocuticle). These tubules (ca. 1 μm diameter) have a high density of 1.5×10^5 mm^{-2} and transport ions

that are critical for forming a new exoskeleton when the animal molts.[87] The tubules enhance the toughness for loading in the direction normal to the exoskeleton surface, by holding together the layered Bouligand structured exo- and endocuticles through ductile interfaces.

An important subset of tubular structures is cylindrical-crossply or Haversian structures. These structures are characterized by cylindrical cross-plies, layered around a tubule, and thus provide additional fracture toughness by acting as uncracked ligaments that shield stresses.[79,94] These Haversian structures are commonly found in mammalian bone.[79,94,95]

7. Cellular Structures

Cellular structures include open and closed cell foams, scaffolds, or other highly porous materials (e.g., honeycombs) (**Figure 8**a), resulting in high-strength–low-weight structures, capable of resisting buckling and bending and/or increasing toughness. Given their weight savings, cellular structures are commonly observed in birds and other flying organisms. However, many terrestrial and marine organisms also contain some form of cellular structures to reduce weight in otherwise dense materials (e.g., bone, shell). Cellular structures can exist as nano- to microstructural elements within a biological composite material or as the macrostructure of a bulk biological material. Specific examples include porcupine quills (Figure 8b),[96] toucan beaks (Figure 8c),[97,98] turtle shells (Figure 8d),[99] antlers (Figure 8e),[8,25] bird bones (Figure 8f),[9] horseshoe crab shells (Figure 8g),[8] and mammalian trabecular bone.[11,25]

Mechanically, cellular structures provide some strength while minimizing weight. There are two general classes of cellular solids: open cell, where there are interconnected pathways that traverse the individual pores of the foam or scaffold, and closed cell, where the individual pores are completely isolated. In general, a relative density, ρ^*/ρ_s, (where ρ^* is the measured density of the cellular scaffold and ρ_s is the density of a fully dense solid of the same material) differentiates open cell ($\rho^*/\rho_s < 0.3$) from closed cell ($\rho^*/\rho_s > 0.3$).[9] Gibson and Ashby[102–104] showed that the relative stiffness of a cellular structure, E^*/E_s, (where E^* is the measured stiffness of the cellular scaffold and E_s is the stiffness of a fully dense solid of the same material) can be determined for open cell (Equation (14)) structures and closed cell (Equation (15)) structures as functions of the material properties:

$$\frac{E^*}{E_s} \approx \left(\frac{\rho^*}{\rho_s}\right)^n \tag{14}$$

where n is a power exponent ranging from 1 to 3 that relates to the stiffness of the material (in biological materials; n approaches 3 for heavily mineralized materials and 1 for unmineralized materials),[9] and:

$$\frac{E^*}{E_s} = \phi^2\left(\frac{\rho^*}{\rho_s}\right)^n + (1-\phi)\frac{\rho^*}{\rho_s} + \frac{P_0(1-2\nu^*)}{E_s\left(1-\frac{\rho^*}{\rho_s}\right)} \tag{15}$$

where ϕ is the fraction of edges within the closed cell of the cellular solid, ν^* is the measured Poisson's ratio and P_0 is the gas pressure within the closed pores. Unlike open-cell structures, closed-cell cellular structures result in numerous enclosed chambers that act as pressure vessels. As a result, the gas pressure and Poisson's ratio must be taken into account. Mechanically, both open- and closed-cell cellular structures result in a unique stress–strain behavior with an initial linear region (due to cell-wall bending), an uneven, jagged plateau region (due to cell-wall buckling and fracture) and finally a sharp increase in modulus (due to cellular densification).[102,104] These expressions demonstrate that the elastic modulus is very sensitive to the amount of porosity. While the majority of biological cellular structures have low relative densities (ca. 10–20%),[103] some such as corals can range between 30 and 50%,[26] and sandwich structures such as turtle shell (ca. 50%)[99] are much denser.

Cellular structures are most commonly surrounded by dense walls, forming sandwich structures. Sandwich structures themselves can be considered composites of two phases: the dense shell and the cellular core. There is often a synergism between the cellular interior and the dense walls. As a result, the mechanical properties of sandwich structures are superior to those predicted from a simple rule-of-mixtures. Gibson and Ashby[102] determined a constitutive equation for the bending compliance of panel-shaped sandwich structures:

$$\left(\frac{\delta}{P}\right) = \frac{2}{B_1 E_f b\left(\frac{t}{L}\right)\left(\frac{c}{L}\right)^2} + \frac{1}{B_2 b\left(\frac{c}{L}\right)G_c^*} \tag{16}$$

where δ is the deflection of the structure, P is the applied load, B_1 and B_2 are constants based upon the loading geometry (see Gibson[103] for more details), b is the width of the structure, t and c are the thickness of the dense shell and porous core respectively, L is the span, E_f is the Young's modulus of the dense shell, and G_c^* is the shear modulus of the core (cellular) material. The first and second terms represent the compliance of the dense shell sections and porous core respectively. These panel-shaped structures can be found in a number of biological materials, such as turtle (Figure 8d)[99] and horseshoe crab shells (Figure 8g).[8] The internal porous material of the sandwich structure serves to lighten the structure and to absorb energy from bending and crushing attacks (Figure 8h).

Cylindrical sandwich structures are very common in nature, consisting of a dense cylinder filled with a porous or foam core. These structures can be found in porcupine quills (Figure 8b),[96,24] mammalian bones and antlers (e.g., elk, Figure 8e),[25] bird bones and feathers (Figure 8f),[9] the toucan beak,[98,105] and plant stems.[41] Cylindrical sandwich structures provide resistance to local bulking in order to avoid premature failure. Filling of a hollow structure with a foam, at a constant weight, significantly increases the bending moment at which buckling is initiated because the walls of the shell are supported. It has been experimentally shown that the critical buckling strength of cylindrical sandwich porcupine quills is increased by up to three times over hollow porcupine quills, holding the weight per unit length constant.[96] This has also been shown for the toucan beak[98] and peacock feathers.[106] Karam and Gibson[107] developed a constitutive equation for the

Adv. Mater. 2015,
DOI: 10.1002/adma.201502403

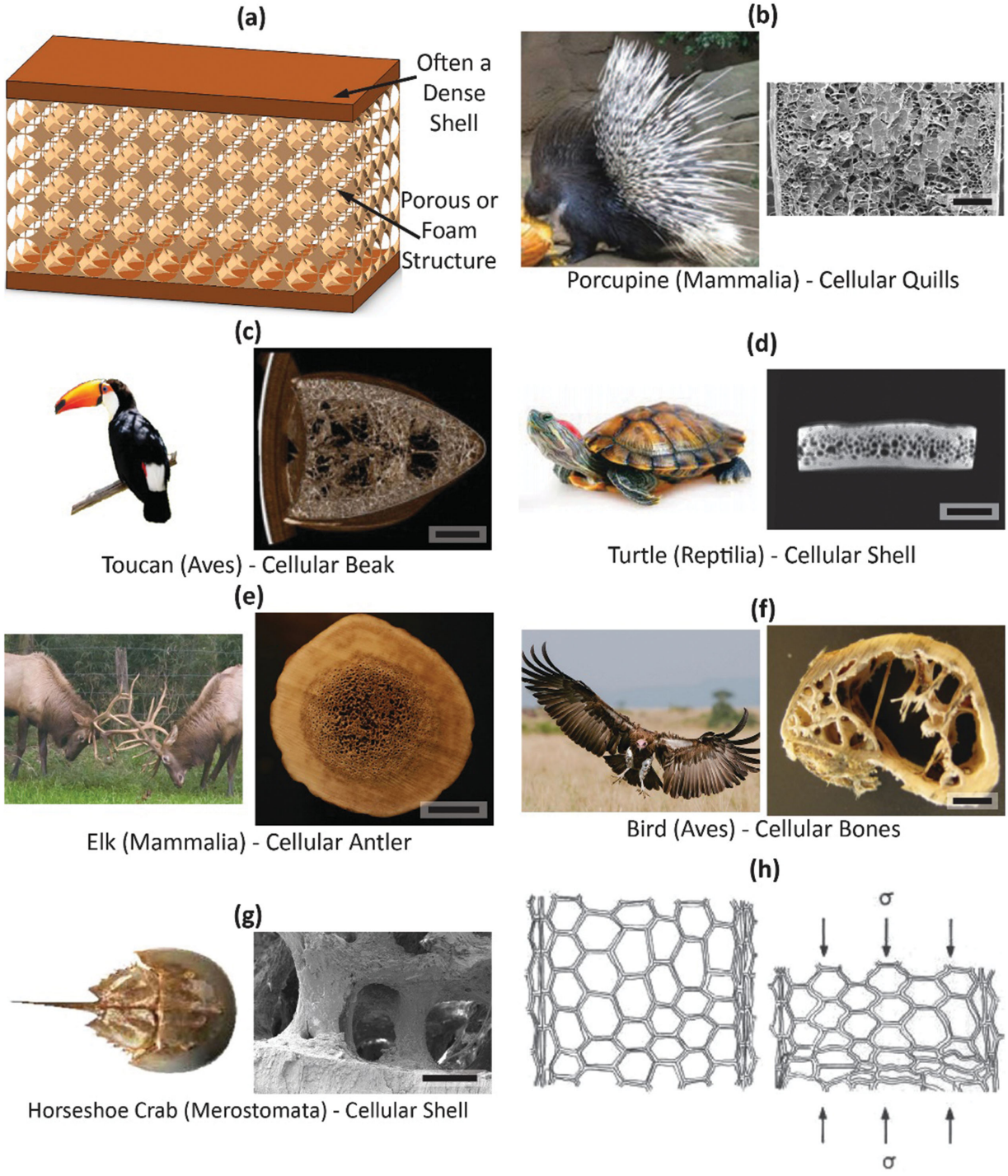

Figure 8. Biological cellular structures from nature representing a variety of biological classes. a) Diagram of a cellular structure displaying a porous or foam structure that is often surrounded by a dense shell; b) Old world porcupine (Mammalia) with foam-filled, cellular quills; c) Toucan (Aves) with a foam-filled, cellular beak; d) Turtle (Reptilia) with a cellular shell; e) Elk (Mammalia) with cellular antlers; f) Birds (Aves) with cellular bones, showing struts extending through the interior and ridges, which add thickness locally; g) Horseshoe Crab (Merostomata) with a cellular shell; h) Diagram of a cellular foam structure under compression showing how the structure buckles and compresses in order to increase deformation and toughness. Scale bars: 500 μm (b), 1 cm (c), 2 mm (d), 10 mm (e), 2 mm (f), 500 μm (g). b) Adapted with permission.[41] Copyright 2013, The American Association for the Advancement of Science (left) and adapted with permission.[24] Copyright 2013, Elsevier (right); c) Adapted with permission.[100] Copyright 2011, Elsevier (left) and adapted with permission.[41] Copyright 2013, The American Association for the Advancement of Science (right); d) Adapted with permission.[9] Copyright 2012, Elsevier (left) and adapted with permission.[99] Copyright 2009, Elsevier (right); e) Adapted with permission.[25] Copyright 2009, Elsevier (left) and adapted with permission.[8] Copyright 2008, Elsevier (right); f) Adapted with permission.[101] Copyright 2013, Nature Publishing Group (left) and graciously donated by E. E. Novitskaya (right); g,h) Adapted with permission.[8] Copyright 2008, Elsevier.

local compressive buckling stress in the longitudinal direction, σ_{cr}, of such structures:

$$\sigma_{cr} = \frac{Et}{a}\left[\frac{1}{12(1-\nu^2)}\frac{a/t}{\left(\lambda_{cr}/t\right)^2} + \frac{\left(\lambda_{cr}/t\right)^2}{\left(a/t\right)} + \frac{2}{(3-\nu_c)(1+\nu_c)}\frac{E_c}{E}\frac{\lambda_{cr}a}{t^2}\right] \quad (17)$$

where E, t, a and ν are the stiffness, thickness, radius, and Poisson's ratio respectively of the dense shell, E_c and ν_c are the stiffness and Poisson's ratio, respectively, of the foam core and $2\lambda_{cr}$ is the wavelength of the instability divided by π, which can be calculated from:

$$\frac{\lambda_{cr}}{t} \approx 0.69\left(\frac{E}{E_c}\right)^{1/3} \quad (18)$$

The buckling strength is a complex function of the geometry and materials properties. Specifically, the critical buckling strength increases as t/a increases; however, in competition, the weight also increases with this ratio. Karam and Gibson[107,108] have reported on the ratios where strength is maximized and weight is minimized for a variety of materials.

Not all cellular structures take on such a simplified structure. One of the most notable and more complex examples of cellular biological structural materials are avian wing bones. Birds have lightweight skeletons, which, coupled with a high lift-to-weight ratio, makes flight possible. Their pulmonary system is complex; many have pneumatic bones (particularly the proximal bones: humerus and femur) that are directly connected to the respiratory system, thereby increasing buoyancy.[109–111] Bird bones are characterized by a much thinner sheath of cortical bone, compared to terrestrial animals.[112] Bones of flying birds need to be strong and stiff enough to withstand forces during takeoff and landing, which necessitates some reinforcement in the bone interior. Wing bones have to resist both bending and torsion forces, as they are rarely loaded in pure tension or compression. Such structures can be modeled as hollow cylinders. The bending stress acting on a thin-walled hollow cylinder can be approximated as:[113]

$$\sigma = \frac{MR}{I} \sim \frac{M}{\pi R^2 t} \quad (19)$$

where M is the bending moment, R is the external radius, I is the second moment of inertia and t is the wall thickness. Similarly, the shear stress (in torsion) of thin-walled hollow cylinders can be determined:[113]

$$\tau = \frac{TR}{J} \sim \frac{T}{2\pi R^2 t} \quad (20)$$

where T is the torque and J is the polar moment of inertia. Both expressions indicate that increasing the wall thickness decreases both torsional and bending stresses, at the expense of an increase in weight. These external forces have necessitated the development of reinforcing structures (struts and ridges) inside the bones (Figure 8f in a turkey-vulture humerus),[110,114] instead of uniformly thickening the wall. Struts appear as reinforcing structures that extend through the center of the bone at places "in need," working against extensive bending forces and preventing ovalization and buckling of bone walls. Ridges occur on the walls and add material locally, thereby increasing both I and J.[114]

8. Suture Structures

Suture structures are wavy or interdigitating interfaces that are found within a variety of plates, scutes, and bones, and generally consist of two phases: rigid suture teeth and a compliant interface layer (**Figure 9**a). They often appear in regions where there is a need to control the intrinsic strength and flexibility of a material interface. Sutures occur as microstructural interfacial elements in biological materials. Specific examples where sutures appear include the carapace of the red-eared slider (Figure 9b)[28] and leatherback turtles,[115] mammalian skulls (e.g., white-tailed deer, Figure 9c),[116,117] the pelvis of threespine sticklebacks (Figure 9d),[118] boxfish scute junctions (Figure 9e),[27] the exoskeletal surfaces (called frustules) of diatoms (Figure 9f),[119] armadillo osteoderms (Figure 9g),[120] and ammonite shells.[121]

Mechanically, suture structures provide strength at the interfaces of rigid biological components while still controlling the flexibility. Li, Ortiz and Boyce[121,123,29,124] have developed a number of constitutive equations for the effective strength of a sutured interface of arbitrary geometry, the most generalized of which, a single repeating triangular suture, is reported here. For this generalized case, it is assumed that two failure modes are possible: tooth failure where the suture teeth themselves fracture, and interface shear failure where a crack propagates through the interface itself around the suture teeth. For an idealized loading situation (loading in tension with the loading axis perpendicular to the sutured interface where the stress is uniform through both the rigid sutures and compliant interface), a critical suture tooth angle, $2\theta_0$, can be determined, where the suture teeth and interface would simultaneously fail, thus creating a strength-optimized structure:[123]

$$2\theta_0 = \sin^{-1}\frac{2\tau_0^f}{\sigma_1^f}, \theta_0 \le \frac{\pi}{4} \quad (21)$$

where τ_0^f is the critical shear stress that would cause shear failure of the interface and σ_1^f is the critical tensile stress that would cause failure of the suture teeth. Note that this equation is reorganized and plotted in Figure 9h to display the strength-optimized boundary between the two failure modes noted above. For any arbitrary suture tooth angle, θ, $\theta \le \theta_0$ will result in a tooth failure while $\theta > \theta_0$ will result in an interface shear failure.

The effective stiffness of a sutured interface, $\overline{E}$, can be calculated as a function of material and geometric parameters:[123]

$$\frac{\overline{E}}{E_1} = \frac{f_v^2}{(1-f_v)\left(\frac{E_1}{G_0}\sin^2\theta\cos^2\theta + \frac{E_1}{E_0}\sin^4\theta\right) + f_v} \quad (22)$$

where E_1 and E_0 are the Young's moduli of the suture teeth and interface phases respectively, G_0 is the shear modulus of

Adv. Mater. 2015,
DOI: 10.1002/adma.201502403

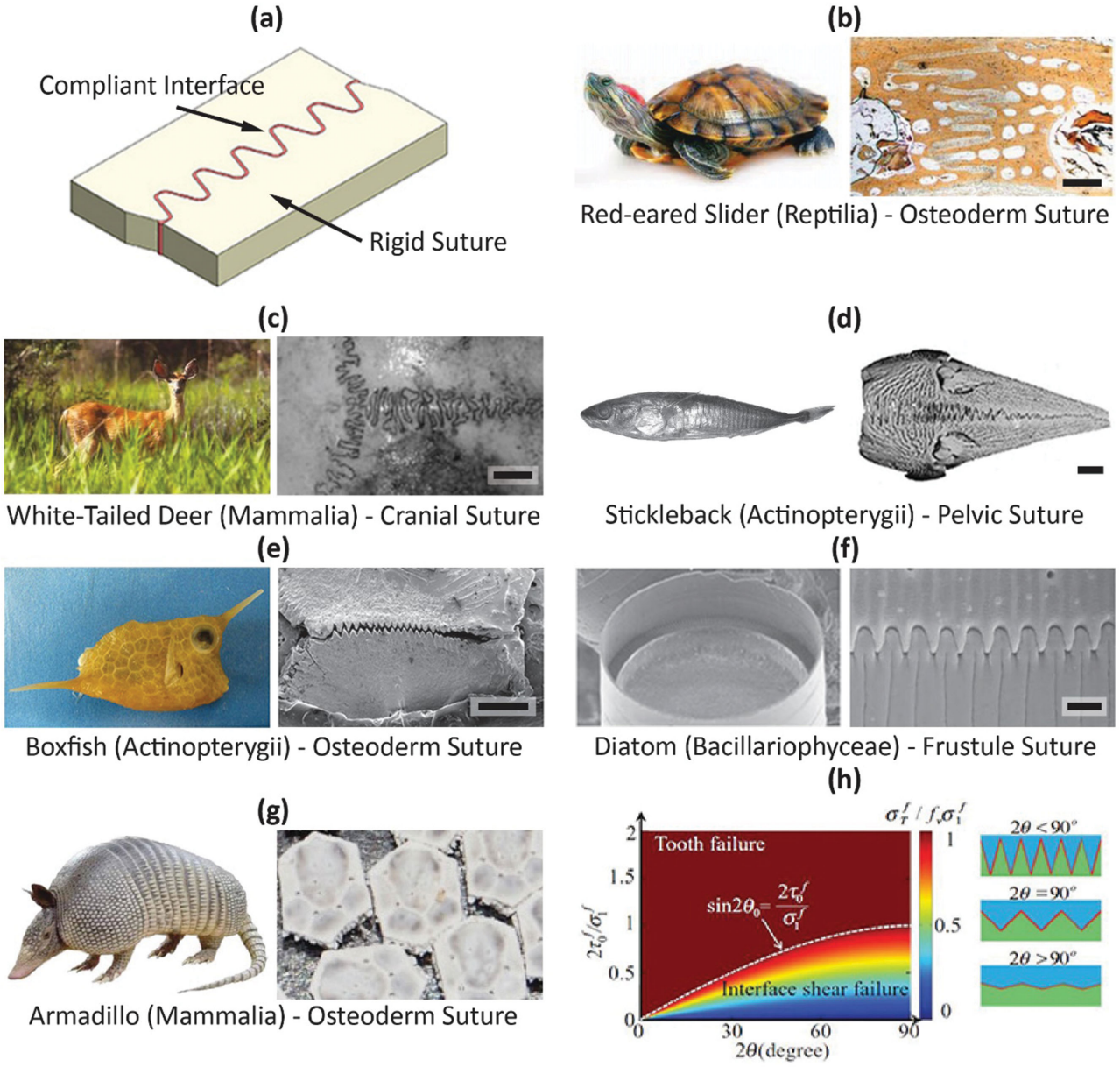

Figure 9. Biological suture structures from nature representing a variety of biological classes. a) Diagram of sutured interfaces displaying the rigid sutures and a compliant interface; b) Red-eared slider (Reptilia) with osteoderm sutures; c) White-tailed Deer (Mammalia) with cranial sutures; d) Stickleback (Actinopterygii) with a pelvic suture; e) Boxfish (Actinopterygii) with scute sutures; f) Diatom (Bacillariophyceae) with exoskeletal (frustule) sutures; g) Armadillo (Mammalia) with osteoderm sutures; h) Mechanical model of the failure mode of triangular suture interfaces based upon the angle of the suture displaying that the maximum strength will occur when the failure modes of tooth and interface shear failure are balanced. Scale bars: 1 mm (b), 1 cm (c), 1 mm (d), 500 μm (e), 1 μm (f). b) Adapted with permission.[9] Copyright 2012, Elsevier (left) and adapted with permission.[28] Copyright 2008, John Wiley and Sons (right); c) Adapted with permission.[122] Copyright 2005, The American Association for the Advancement of Science (left) and adapted with permission.[116] Copyright 2006, John Wiley and Sons (right); d) Adapted with permission.[118] Copyright 2010, Elsevier; e) Adapted with permission.[27] Copyright 2015, Elsevier; f) Adapted with permission.[119] Copyright 2003, John Wiley and Sons; g) Adapted with permission.[9] Copyright 2012, Elsevier (left) and adapted with permission.[120] Copyright 2011, Elsevier (right); h) Adapted with permission.[123] Copyright 2011, American Physical Society.

the interface phase, and f_v is a non-dimensional suture phase volume fraction:[123]

$$f_v = \frac{(\lambda - 2g)}{\lambda} \tag{23}$$

where λ is the wavelength of the suture teeth and g is the thickness of the interface layer. These equations, though for an idealized state, allow for basic understanding of the optimized geometry of suture structures. As an example, Li et al.[123] presented a case for a bone-like suture structure ($f_v = 0.8$) where the suture

teeth are assumed to be bone (E_1 = 10 GPa, σ_1^f = 100 MPa) and the interface is collagen (E_0 = 100 MPa, τ_0^f = 20 MPa). With these conditions, the strength-optimized suture tooth angle is $2\theta_0 = 23.6°$. Of note, the experimentally measured sutures of bone-like biological structures in red-eared slider turtles (2θ = 9.4–22°, Figure 9b),[28] white-tailed deer (2θ = 9–25°, Figure 9c),[29] leatherback sea turtle (2θ = 30°),[115] and three spine stickleback fish (2θ = 6–20°, Figure 9d)[118] are all similar to this predicted optimized angle.

Beyond the simplified suture structures described above, recent work by Lin et al.[124] has shown that increasing the level of hierarchy of a sutured interface can significantly improve the mechanical properties. A suture structure with a high level of hierarchy (e.g., deer cranial sutures, Figure 9c) will generally have higher stiffness and toughness than a simple suture (e.g., diatom frustule sutures (Figure 9f), or boxfish scute sutures (Figure 9e)). In addition, the design and level of hierarchy can effectively tailor the tensile strength.

9. Overlapping Structures

Overlapping structures are composed of a number of individual plates or scales that can slide or shift past each other, forming a flexible protective surface (**Figure 10**a). These are most commonly employed as armor. Overlapping structures occur as macrostructural elements. Specific examples include seahorse tails (Figure 10b),[30] shark skin (Figure 10c),[125] the millipede exoskeleton (Figure 10d),[126] the chiton exoskeleton (Figure 10e),[32] fish scales (e.g., alligator gar (Figure 10f) and arapaima),[3,22,127] and pangolin plates (Figure 10g).[9]

Mechanically, overlapping structures are capable of ensuring constant coverage while allowing flexibility. Vernerey and Barthelat[130–132] have developed an analytical model to describe how the individual scales or plates of an overlapping structure contribute to the total curvature. These equations were specifically designed with a focus on the scales of fish; however, they provide valuable insight into most overlapping structures. The normalized curvature of the entire overlapping structure is expressed as $\bar{\kappa} = \ell / R$, where l is the projected length of a scale (given that all scales, in an undeformed state are raised from the dermal surface by a small angle) and R is the radius of curvature of the entire articulated body. The normalized curvature, $\bar{\kappa}$, is composed of two separate terms:[130]

$$\bar{\kappa} = \bar{\kappa}_r + \bar{\kappa}_b \tag{24}$$

where $\bar{\kappa}_r$ is the normalized curvature due to rotation of the scales at the proximal end and $\bar{\kappa}_b$ is the normalized curvature due to bending of the individual scales. Combined, these two terms account for the ability of the articulated scales to conform to R with the assumption that the bending of the scales is relatively small ($\bar{\kappa}_b < 0.1$). This assumption is valid for most biological scales and plates, which are often rigid due to mineral reinforcements, causing the contribution of scale rotation to dominate. With this in mind, the angle, θ, at which each scale must rotate to accommodate a given $\bar{\kappa}_r$ can be determined:[130]

$$\theta = -\frac{\beta}{2} + \sin^{-1}\left[\bar{\kappa}_r \cos\left(\frac{\beta}{2}\right)\right] \tag{25}$$

where β is the angle between the distal ends of two adjacent scales when the body is in a curved state. This angle can also be expressed for any given body curvature as $\beta = s/R$ where s is the scale spacing between the proximal ends of two adjacent scales. Any remaining curvature is attributed to $\bar{\kappa}_b$, which given the previously discussed assumption, should be small.

Given that the rotation at the proximal end of embedded scales and plates, θ, is the primary mode of flexing, the variables in Equation (25) provide insight into the important qualities of an overlapping structure that ensure both flexibility and full protection. The dominant independent variables are the scale length (effectively l, found within $\bar{\kappa}_r$), the spacing between scales (s, found within β) and the total body length (that influences R, found within $\bar{\kappa}_r$). Most organisms employ scales that balance these variables/qualities, providing high overall flexibility (R) to facilitate natural motion while minimizing the local rotation of scales (θ) to resist puncture (Figure 10h). This is accomplished by reducing the ratio of scale size to body length (minimizing s and $\bar{\kappa}$). Overlapping structures based on these characteristics are common in many fish such as sharks (Figure 10c),[125] arapaima,[3,53] Senegal bichir,[63] striped-bass[55,133] and alligator gar (Figure 10f),[22] and the majority of teleosts, as well as pangolin (a mammal) (Figure 10g).[9] However, a number of fish (e.g., syngnathids; Figure 10b) have also evolved modified overlapping structures (e.g., peg-and-socket connections) designed for specific functions, such as grasping.[30,134–136] Although the geometries and resulting mechanics of the different overlapping structures can vary significantly among species, these plated structures provide all organisms some level of combined strength and flexibility.

10. Bioinspired Design

Synthetic materials that mimic one or more of the eight structural design elements have been developed in recent years using many different materials processing routes. With the advent of modern biotechnology and nanoscale manufacturing, hierarchical materials (or composites) composed of ceramics and/or polymers are now becoming viable alternatives to the other dominant class of structural materials: metals. Such ceramic- and polymer-based materials are lightweight and exhibit impressive mechanical properties in spite of their relatively low densities; in many cases, this is the direct result of including the aforementioned structural design elements. **Figure 11** provides a few representative examples of different bioinspired materials that utilize these structural design elements for enhanced mechanical performance. For more comprehensive reviews on these and other bioinspired materials, refer to refs.[9,137] This cornucopia of materials (Figure 11) highlights a range of techniques used to fabricate architectures at the micro-, meso- and macroscales, including: recombinant technologies, biomineralization, layer-by-layer deposition, self-assembly, bio-templating, magnetic manipulation, freeze-casting, vacuum-casting, extrusion and roll compaction, laser engraving, and 3D-printing (additive manufacturing).

Bioengineered synthetic fibrous structures (Figure 11a) have been developed from recombinant spider silks (proteins), via genetic manipulation of mammalian cells,[138] and metabolically

DOI: 10.1002/adma.201502403

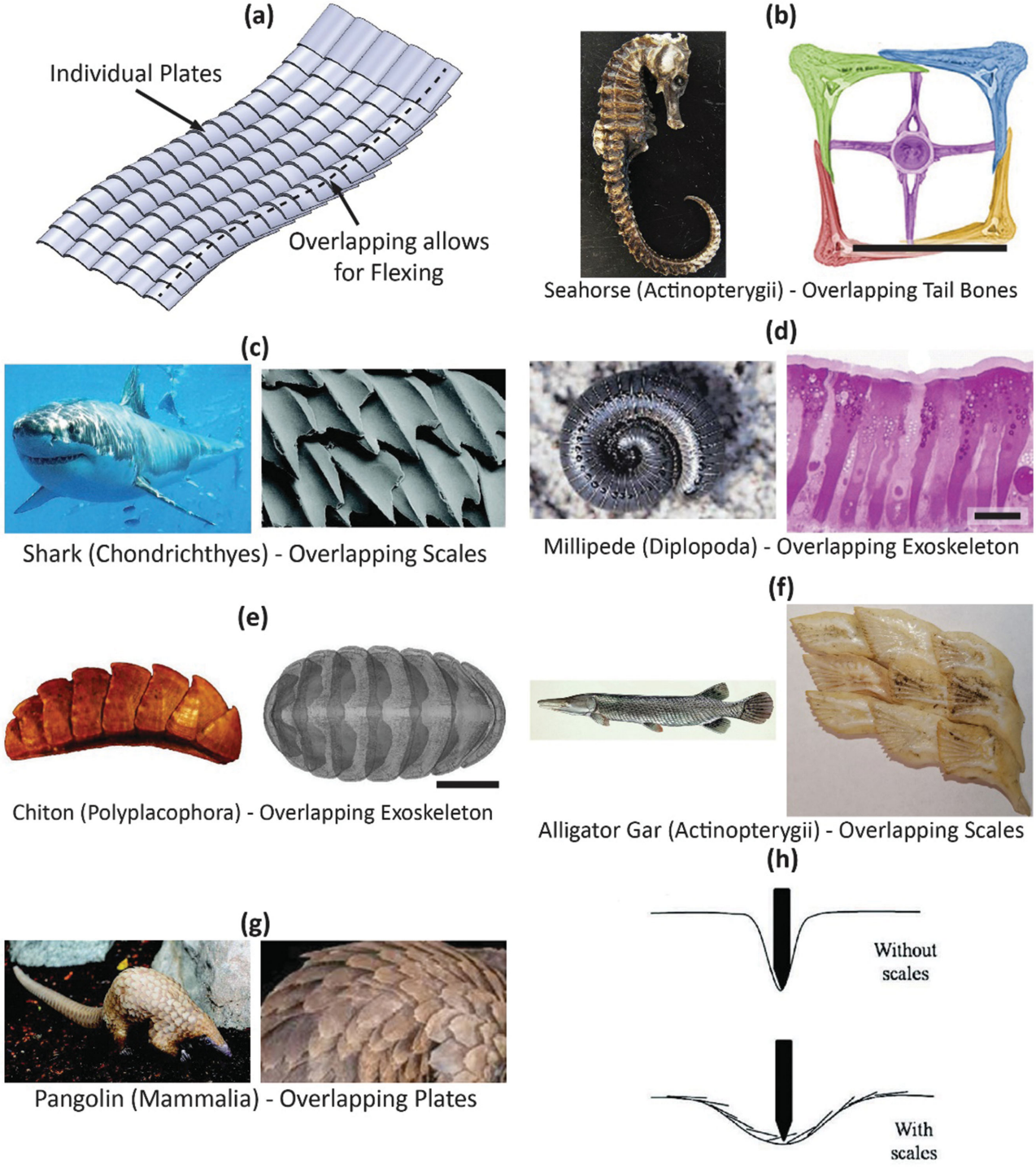

Figure 10. Biological overlapping structures from nature representing a variety of biological classes. a) Diagram of overlapping structures that are made of individual plates and allow for flexing while ensuring full coverage; b) Seahorse (Actinopterygii) with overlapping bony tail plates; c) Shark (Chondrichthyes) with overlapping scales; d) Millipede (Diplopoda) with an overlapping exoskeleton; e) Chiton (Polyplacophora) with an overlapping exoskeleton; f) Alligator gar (Actinopterygii) with overlapping scales; g) Pangolin (Mammalia) with overlapping plates; h) Diagram demonstrating how the use of overlapping scales defends against penetration. Scale bars: 5 mm (b), 15 μm (d), 50 mm (e). b) Adapted with permission.[30] Copyright 2013, Elsevier; c) Adapted with permission.[128] Copyright 2008, Nature Publishing Group (left) and adapted with permission.[125] Copyright 2012, John Wiley and Sons (right); d) Adapted with permission.[129] Copyright 1998, Nature Publishing Group (left) and adapted with permission.[126] Copyright 2014, Elsevier (right); e) Adapted with permission.[32] Copyright 2012, Elsevier; f) Adapted with permission.[22] Copyright 2013, Elsevier (left) and graciously donated by V. Sherman (right); g) Adapted with permission.[9] Copyright 2012, Elsevier (left) and adapted with permission.[125] Copyright 2012, John Wiley and Sons (right); h) Adapted with permission.[125] Copyright 2012, John Wiley and Sons.

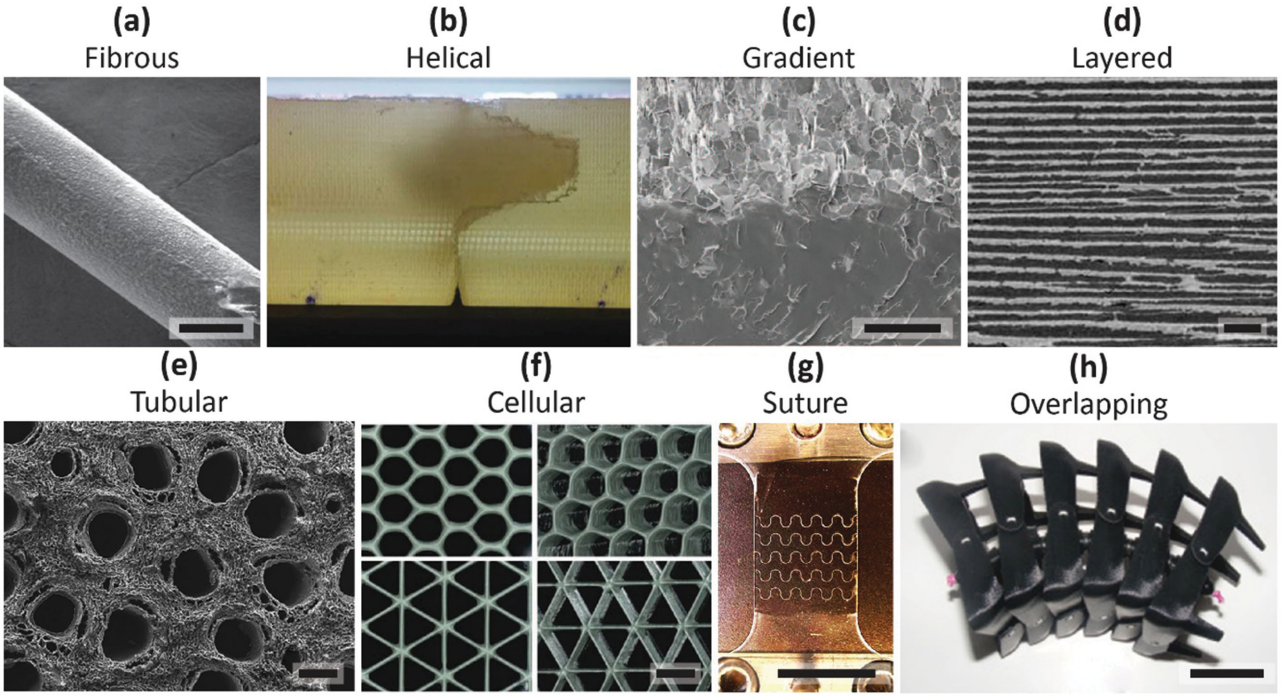

Figure 11. Examples of bioinspired designs for each of the eight structural design elements. a) Fibrous recombinant spider silk from mammalian cells; b) helical fiber reinforced composites that are capable of deflecting crack growth; c) gradient structures formed by applying magnetic fields to a particle-reinforced matrix composite; d) layered composites formed from freeze casting; e) tubules formed from bio-templating; f) 3D-printed cellular structures; g) sutures employed to toughen glass; h) overlapping structures for potential robotics. Scale bars: 5 μm (a), 40 μm (c), 100 μm (d), 250 μm (e), 2 mm (f), 8 mm (g), 25 mm (h). a) Adapted with permission.[138] Copyright 2002, The American Association for the Advancement of Science; b) Graciously donated by D. Kisailus; c) Adapted with permission.[139] Copyright 2012, The American Association for the Advancement of Science; d) Adapted with permission.[140] Copyright 2008, The American Association for the Advancement of Science; e) Adapted with permission.[141] Copyright 2009, Royal Society of Chemistry; f) Adapted with permission.[142] Copyright 2014, John Wiley and Sons; g) Adapted with permission.[143] Copyright 2014, Nature Publishing Group; h) Adapted with permission.[134] Copyright 2015, The American Association for the Advancement of Science.

engineered bacterial cells.[144] The resulting proteins can be spun into fibers that exhibit tensile properties comparable to native dragline silks with high strengths up to 1.1 GPa.[145] In addition, the use of self-assembly techniques has proven to be an effective method of creating nanoscale bioinspired fibers.[146] Similar fiber-based designs have been employed to mimic helical structures. As an example, carbon-fiber–epoxy composites arranged into helicoidal architectures (Figure 11b), akin to naturally occurring Bouligand structures, were recently shown to exhibit enhanced impact resistance, as compared to unidirectional and quasi-isotropic controls (industry standards).[147] The damage mechanisms observed in these fiber composites resembled those observed in the stomatopod dactyl club,[16,148] where crack propagation follows the path of least resistance, forcing damage to spread in-plane rather than through the thickness of the helicoidal composites. The use of magnetic fields to manipulate or align the internal microstructures of materials is another simple method to create bioinspired designs, as demonstrated on polymer–matrix composites (Figure 11c) where embedded particles with varying morphologies (e.g., platelets or rods) are aligned with a magnetic field to create gradient structures with localized properties and three-dimensional reinforcement.[139]

Other common synthetic processing techniques used in bioinspiration are those that employ natural phenomena (e.g., ice) as a template. These techniques are gaining popularity due to their ease of use and relatively low environmental impact. Freeze-casting (or ice-templating) is one such process that harnesses the unique crystallographic properties of ice to grow columnar channels within an aqueous slurry of particles (typically ceramic powders). The resulting material is a scaffold with interconnected pores that replicate the structural organization of the ice.[140,149] Upon removal of the ice, the scaffolds may be subjected to a variety of post-processing methods (e.g., polymer infiltration and/or sintering) to fabricate materials with layered microstructures (Figure 11d). This technique has been remarkably successful for making layered composites that closely mimic the brick-and-mortar architecture of abalone nacre, leading to some of the toughest ceramic-based materials known to date.[140,150] Adding magnetic fields to the freeze-casting process has also been shown to make materials with gradient[151] and helical[60] architectures. The use of layer-by-layer deposition through sequential absorption of oppositely charged materials into a substrate,[152] the extrusion and roll compaction of alternating layers of materials,[152] and the self-assembly of polymer-coated nanolayers[153] are also effective techniques for the creation of bioinspired layered structures. The use of other natural materials (e.g., wood) to act as a sacrificial template, which may be loosely referred to as bio-templating,

Adv. Mater. **2015**,
DOI: 10.1002/adma.201502403

has been investigated for the design and fabrication of similar structures composed of different material constituents (e.g., hydroxyapatite minerals). This technique has been used to replicate already-existing natural structures, such as the tubular structures present in native rattan and pine woods, into chemically engineered materials composed of hydroxyapatite (the primary mineral constituent of bone) for the development of porous bone implants (Figure 11e).[141]

In contrast to these templating methods, the use of modern technology has given rise to a number of accurate and directed fabrication techniques that allow for the creation of materials in a predefined user-controlled fashion. This allows for the fabrication of designer materials with intricate internal (and external) structures and properties.[142] The technique of 3D-printing has been prolifically employed for the creation of bioinspired cellular structures (Figure 11f).[142] Similarly, the accuracy of laser etching has been employed to explore the effects of controlled geometry in structures.[143] Brittle glass was toughened by engraving tiny defects into suture patterns that guide cracks through jigsaw-like interfaces (Figure 11g). This allowed for predefined control of crack propagation, leading to a bioinspired glass that is up to 200 times tougher than a non-engraved glass.[143] Finally, this high control of structure forming has allowed for the fabrication of more-complex mimetic structures such as the overlapping skeleton of a seahorse tail for potential robotics applications (Figure 11h).[134]

11. Conclusions and Summary

The current wave of investigations on biological materials using the computational, experimental and analytical tools of materials science is rapidly expanding our knowledge, but presents a dazzling complexity that poses a challenge to inquiry. The current lack of a simple framework with which to characterize these structures complicates the sharing of knowledge within the scientific community. It is for this reason that we are proposing a new paradigm rooted in eight structural-design elements: fibrous, helical, gradient, layered, tubular, cellular, suture, and overlapping structures.

- Fibrous structures provide high tensile, but effectively no compressive resistance and are employed within a wide variety of silks, muscles and connective tissues (e.g., hagfish slime, spider silk).
- Helical structures can be either a twisted ply that provides in-plane isotropy and increased toughness, or reinforcements that provide torsional rigidity. As a result, helical structures are found in a wide variety of structural and protective materials (e.g., crab and insect exoskeletons).
- Gradient structures occur at material interfaces and accommodate property mismatch through a gradual transition. They provide increased toughness and are predominately found linking rigid and compliant materials in teeth, protective scales, and exoskeletons.
- Layered structures increase the toughness of, most commonly, brittle materials through the introduction of numerous interfaces, and are found through a variety of support structures (e.g., mollusk nacre, sponge spicules).
- Tubular structures employ organized cylindrical porosity in order to increase toughness, through either energy absorption, crack deflection, or wave scattering. They are found in protective materials that are designed to absorb impact, such as hooves, horns, and teeth.
- Cellular structures consist of porous materials or foams that allow for stress distribution and energy absorption while minimizing weight. They are often surrounded by dense layers in order to form sandwich structures. Cellular structures are found in a wide variety of organisms (e.g., turtle shells, porcupine quills).
- Suture structures are wavy and interdigitating interfaces that provide control of the strength and flexibility. They are found in protective structures and can be tailored to either provide more flexibility (e.g., leatherback sea turtles, sticklebacks) or stiffness (e.g., mammalian skulls).
- Overlapping structures provide for flexibility while ensuring complete coverage of the body. They are found in a variety of protective exteriors from the exoskeletons of millipedes to the scales of fish.

It is proposed that current and novel discoveries of structural elements within biological materials should all, in some way, be characterized into these design elements. Of important note, many biological materials exhibit two or more of these structural elements that cooperate to provide a complex array of multifunctional properties for the organism. Examples include the lobster endocuticle, stomatopod dactyl club, and bird feathers. The endocuticle of the lobster consists of a helical bulk (a twisted plywood arrangement of mineralized chitin fibers) along with tubular structures.[154] The combination of these allows for enhanced properties where, in certain loading modes, the tubules can improve resistance against delamination of the helical fibers.[154] The stomatopod's dactyl club combines a gradient structure at the outer surface (to resist crack propagation) with a helical structure within its bulk (to dissipate energy) in order to enable the impacts of its incredible natural punching behavior.[16] Bird feathers combine a cellular core along with helical fiber walls to form a reinforced sandwich structure that provides increased flexure and torsion resistance.[100] The identification of these design elements provides a rational basis for the understanding of the mechanical properties of structural biological materials. In each case, these design elements provide specific mechanical and structural advantages. Knowledge of these advantages has already led to significant research and development in the field of bioinspired design. Further research into the function of each of these design elements will only lead to bioinspired designs that are more efficient and effective, allowing for our understanding of biological materials and the natural world to have a positive impact on society.

Acknowledgments

This work was supported by a Multi-University Research Initiative through the Air Force Office of Scientific Research (AFOSR-FA9550–15–1–0009) (S.E.N., M.A.M., and J.M.) and by the Department of Mechanical Engineering, Clemson University (M.M.P.). Discussions with Profs.

Horacio Espinosa, David Kisailus, Phil Hastings, Jennifer R. A. Taylor, Robert O. Ritchie, and Dominique Adriaens are gratefully acknowledged. Additionally, the authors wish to acknowledge the participation and advice of Dr. Wen Yang, Dr. Katya Novitskaya, Jae-Young Jung, Michael B. Frank, Bin Wang, Vincent Sherman, Frances Su and Kate C. Fickas.

Received: May 19, 2015
Revised: June 16, 2015
Published online:

[1] C. Mora, D. P. Tittensor, S. Adl, A. G. B. Simpson, B. Worm, *PLoS Bio.* **2011**, *9*, e1001127.
[2] S. Weiner, W. Traub, H. D. Wagner, *J. Struct. Biol.* **1999**, *126*, 241.
[3] Y. S. Lin, C. T. Wei, E. A. Olevsky, M. A. Meyers, *J. Mech. Behav. Biomed. Mater.* **2011**, *4*, 1145.
[4] F. Barthelat, H. Tang, P. D. Zavattieri, C. M. Li, H. D. Espinosa, *J. Mech. Phys. Solids* **2007**, *55*, 306.
[5] R. Menig, M. H. Meyers, M. A. Meyers, K. S. Vecchio, *Acta Mater.* **2000**, *48*, 2383.
[6] F. Barthelat, H. D. Espinosa, *Exp. Mech.* **2007**, *47*, 311.
[7] J. Aizenberg, J. C. Weaver, M. S. Thanawala, V. C. Sundar, D. E. Morse, P. Fratzl, *Science* **2005**, *309*, 275.
[8] M. A. Meyers, P.-Y. Chen, A. Y. M. Lin, Y. Seki, *Prog. Mater. Sci.* **2008**, *53*, 1.
[9] P.-Y. Chen, J. McKittrick, M. A. Meyers, *Prog. Mater. Sci.* **2012**, *57*, 1492.
[10] S. E. Naleway, J. R. A. Taylor, M. M. Porter, M. A. Meyers, J. McKittrick, unpublished.
[11] J. McKittrick, P.-Y. Chen, L. Tombolato, E. E. Novitskaya, M. W. Trim, G. A. Hirata, E. A. Olevsky, M. F. Horstemeyer, M. A. Meyers, *Mater. Sci. Eng. C* **2010**, *30*, 331.
[12] D. S. Fudge, K. H. Gardner, V. T. Forsyth, C. Riekel, J. M. Gosline, *Biophys. J.* **2003**, *85*, 2015.
[13] V. Ottani, D. Martini, M. Franchi, A. Ruggeri, M. Raspanti, *Micron* **2002**, *33*, 587.
[14] J. A. Kluge, O. Rabotyagova, G. G. Leisk, D. L. Kaplan, *Trends Biotechnol.* **2008**, *26*, 244.
[15] T. Lenau, M. Barfoed, *Adv. Eng. Mater.* **2008**, *10*, 299.
[16] J. C. Weaver, G. W. Milliron, A. Miserez, K. Evans-Lutterodt, S. Herrera, I. Gallana, W. J. Mershon, B. Swanson, P. Zavattieri, E. DiMasi, D. Kisailus, *Science* **2012**, *336*, 1275.
[17] S. Bechtle, T. Fett, G. Rizzi, S. Habelitz, A. Klocke, G. A. Schneider, *Biomaterials* **2010**, *31*, 4238.
[18] B. W. Cribb, A. Rathmell, R. Charters, R. Rasch, H. Huang, I. R. Tibbetts, *Arthopod Struct. Development* **2009**, *38*, 173.
[19] A. Miserez, T. Schneberk, C. J. Sun, F. W. Zok, J. H. Waite, *Science* **2008**, *319*, 1816.
[20] P.-Y. Chen, J. Schirer, A. Simpson, R. Nay, Y.-S. Lin, W. Yang, M. I. Lopez, J. Li, E. A. Olevsky, M. A. Meyers, *J. Mater. Res.* **2012**, *27*, 100.
[21] J. H. Kinney, S. J. Marshall, G. W. Marshall, *Crit. Rev. Oral Biol. Med.* **2003**, *14*, 13.
[22] W. Yang, B. Gludovatz, E. A. Zimmermann, H. A. Bale, R. O. Ritchie, M. A. Meyers, *Acta Biomater.* **2013**, *9*, 5876.
[23] L. Tombolato, E. E. Novitskaya, P.-Y. Chen, F. A. Sheppard, J. McKittrick, *Acta Biomater.* **2010**, *6*, 319.
[24] W. Yang, C. Chao, J. McKittrick, *Acta Biomater.* **2013**, *9*, 5297.
[25] P.-Y. Chen, A. G. Stokes, J. McKittrick, *Acta Biomater.* **2009**, *5*, 693.
[26] S. Hamza, N. Slimane, Z. Azari, G. Pluvinage, *Appl. Surf. Sci.* **2013**, *264*, 485.
[27] W. Yang, S. E. Naleway, M. M. Porter, M. A. Meyers, J. McKittrick, *Acta Biomater.* **2015**, *23*, 1.
[28] S. Krauss, E. Monsonego-Ornan, E. Zelzer, P. Fratzl, R. Shahar, *Adv. Mater.* **2009**, *21*, 407.
[29] Y. Li, C. Ortiz, M. C. Boyce, *J. Mech. Phys. Solids* **2013**, *61*, 1144.
[30] M. M. Porter, E. E. Novitskaya, A. B. Castro-Cesena, M. A. Meyers, J. McKittrick, *Acta Biomater.* **2013**, *9*, 6763.
[31] A. K. Dastjerdi, F. Barthelat, *J. Mech. Behav. Biomed. Mater.* **2015**, DOI: 10.1016/j.jmbbm.2014.09.025.
[32] M. J. Connors, H. Ehrlich, M. Hog, C. Godeffroy, S. Araya, I. Kallai, D. Gazit, M. Boyce, C. Ortiz, *J. Struct. Biol.* **2012**, *177*, 314.
[33] F. Vollrath, *Mol. Biotechnol.* **2000**, *74*, 67.
[34] D. S. Fudge, J. M. Gosline, *Proc. R. Soc. B* **2004**, *271*, 291.
[35] D. S. Fudge, N. Levy, S. Chiu, J. M. Gosline, *J. Exp. Biol.* **2005**, *208*, 4613.
[36] V. R. Sherman, W. Yang, M. A. Meyers, *J. Mech. Behav. Biomed. Mater.* **2015**, DOI:10.1016/j.jmbbm.2015.05.023.
[37] M. Heim, D. Keerl, T. Scheibel, *Angew. Chem.* **2009**, *48*, 3584.
[38] J. McKittrick, P.-Y. Chen, S. G. Bodde, W. Yang, E. E. Novitskaya, M. A. Meyers, *JOM* **2012**, *64*, 449.
[39] S. W. Downing, R. H. Spitzer, W. L. Salo, J. S. Downing, L. J. Saidel, E. A. Koch, *Science* **1981**, *212*, 326.
[40] J. G. Hardy, L. M. Romer, T. R. Scheibel, *Polymer* **2008**, *49*, 4309.
[41] M. A. Meyers, J. McKittrick, P.-Y. Chen, *Science* **2013**, *339*, 773.
[42] A. Gautieri, S. Vesentini, A. Redaelli, M. J. Buehler, *Nano Lett.* **2011**, *11*, 757.
[43] Y. Lanir, *Biophys. J.* **1978**, *24*, 541.
[44] A. D. Freed, T. C. Doehring, *J. Biomech. Eng.* **2005**, *127*, 587.
[45] V. R. Sherman, W. Yang, M. A. Meyers, unpublished.
[46] R. W. Ogden, *Proc. R. Soc. London Ser. A* **1972**, *326*, 565.
[47] E. M. Arruda, M. C. Boyce, *J. Mech. Phys. Solids* **1993**, *41*, 389.
[48] Y. C. Fung, *Biomechanics: Mechanical Porperties of Living Tissues*, 2nd ed., Springer, New York **1993**.
[49] T. Yamamoto, T. Hasegawa, M. Sasaki, H. Hongo, C. Tabata, Z. S. Liu, M. Q. Li, N. Amizuka, *J. Electron Microsc.* **2012**, *61*, 113.
[50] J. C. Weaver, J. Aizenberg, G. E. Fantner, D. Kisailus, A. Woesz, P. Allen, K. Fields, M. J. Porter, F. W. Zok, P. K. Hansma, P. Fratzl, D. E. Morse, *J. Struct. Biol.* **2007**, *158*, 93.
[51] Y. Bouligand, *Tissue Cell* **1972**, *4*, 189.
[52] E. A. Zimmermann, B. Gludovatz, E. Schaible, N. K. N. Dave, W. Yang, M. A. Meyers, R. O. Ritchie, *Nat. Commun.* **2013**, *4*, 2634.
[53] W. Yang, V. R. Sherman, B. Gludovatz, M. Mackey, E. A. Zimmermann, E. H. Chang, E. Schaible, Z. Qin, M. J. Buehler, R. O. Ritchie, M. A. Meyers, *Acta Biomater.* **2014**, *10*, 3599.
[54] A. C. Neville, *Biological Fibrous Composites: Devlopment Beyond the Cell Membrane*, Cambridge University Press, New York **1993**.
[55] D. Zhu, C. F. Ortega, R. Motamedi, L. Szewciw, F. Vernerey, F. Barthelat, *Adv. Eng. Mater.* **2012**, *14*, B185.
[56] G. A. Sword, M. Lecoq, S. J. Simpson, *J. Insect Physiol.* **2010**, *56*, 949.
[57] N. Guarin-Zapata, J. Gomez, N. Yaraghi, D. Kisailus, P. D. Zavattieri, *Acta Biomater.* **2015**, DOI:10.1016/j.actbio.2015.04.039.
[58] M. C. S. Kingsley, M. A. Ramsay, *Arctic* **1988**, *41*, 236.
[59] S. Skatter, B. Kucera, *Holz als Roh- und Werkstoff* **1997**, *55*, 207.
[60] M. M. Porter, L. Meraz, A. Calderon, H. Choi, A. Chouhan, L. Wang, M. A. Meyers, J. McKittrick, *Compos. Struct.* **2015**, *119*, 174.
[61] D. A. W. Thompson, *On Growth and Form,* Cambridge University Press, Cambridge, UK **1917**.
[62] G. Harary, A. Tal, *Comput. Graphics Forum* **2011**, *30*, 237.
[63] B. J. F. Bruet, J. H. Song, M. C. Boyce, C. Ortiz, *Nat. Mater.* **2008**, *7*, 748.
[64] S. Roy, B. Basu, *Mater. Characterization* **2008**, *59*, 747.
[65] S. Suresh, *Science* **2001**, *292*, 2447.
[66] S. Suresh, A. E. Giannakopoulos, J. Alcala, *Acta Mater.* **1997**, *45*, 1307.

[67] I. S. Choi, M. Dao, S. Suresh, *J. Mech. Phys. Solids* **2008**, *56*, 157.
[68] A. E. Giannakopoulos, S. Suresh, *Int. J. Solids Struct.* **1997**, *34*, 2357.
[69] A. E. Giannakopoulos, S. Suresh, M. Finot, M. Olsson, *Acta Metall.* **1995**, *43*, 1335.
[70] A. S. Kim, J. Besson, A. Pineau, *Int. J. Solids Struct.* **1999**, *36*, 1845.
[71] A. S. Kim, S. Suresh, C. F. Shih, *Int. J. Solids Struct.* **1997**, *34*, 3415.
[72] V. Imbeni, J. J. Kruzic, G. W. Marshall, S. J. Marshall, R. O. Ritchie, *Nat. Mater.* **2005**, *4*, 229.
[73] A. Miserez, D. Rubin, J. H. Waite, *J. Biol. Chem.* **2010**, *285*, 38115.
[74] A. Woesz, J. C. Weaver, M. Kazanci, Y. Dauphin, J. Aizenberg, D. E. Morse, P. Fratzl, *J. Mater. Res.* **2006**, *21*, 2068.
[75] P. M. Hughes, *Tissue Cell* **1987**, *19*, 705.
[76] A. Y. M. Lin, M. A. Meyers, K. S. Vecchio, *Mater. Sci. Eng. C* **2006**, *26*, 1380.
[77] T. L. Anderson, *Fracture Mechanics Fundamentals and Applications*, 3rd ed., Taylor & Francis Group, Boca Raton, FL, USA **2005**.
[78] R. K. Nalla, J. J. Kruzic, R. O. Ritchie, *Bone* **2004**, *34*, 790.
[79] M. E. Launey, M. J. Buehler, R. O. Ritchie, *Annu. Rev. Mater. Sci.* **2010**, *40*, 25.
[80] M. E. Launey, P.-Y. Chen, J. McKittrick, R. O. Ritchie, *Acta Biomater.* **2010**, *6*, 1505.
[81] R. O. Ritchie, M. J. Buehler, P. Hansma, *Phys. Today* **2009**, *62*, 41.
[82] R. O. Ritchie, *Int. J. Fract.* **1999**, *100*, 55.
[83] R. O. Ritchie, *Nat. Mater.* **2011**, *10*, 817.
[84] R. Menig, M. H. Meyers, M. A. Meyers, K. S. Vecchio, *Mater. Sci. Eng. A* **2001**, *297*, 203.
[85] M. A. Kasapi, J. M. Gosline, *J. Exp. Biol.* **1997**, *200*, 1639.
[86] M. W. Trim, M. F. Horstemeyer, H. Rhee, H. Le Kadiri, L. N. Williams, J. Liao, K. B. Walters, J. McKittrick, S. J. Park, *Acta Biomater.* **2011**, *7*, 1228.
[87] P.-Y. Chen, A. Y. M. Lin, J. McKittrick, M. A. Meyers, *Acta Biomater.* **2008**, *4*, 587.
[88] J. Whitfield, *Nature* **2003**, DOI:10.1038/news031208-10.
[89] V. A. Lubarda, *Introduction to the Mechanics of Deformable Bodies*, 2nd ed., University of Montenegro Press, Podgorica, Montenegro **1989**.
[90] G. E. Exadaktylos, K. N. Kaklis, *Int. J. Rock Mech. Mining Sci.* **2001**, *38*, 227.
[91] M. A. Kasapi, J. M. Gosline, *Equine Veterinary J.* **1998**, *26*, 10.
[92] C. Ziskind, S. Fleischer, K. Zhang, S. R. Cohen, H. D. Wagner, in: *Advances in Mathematical Modeling and Experimental Methods for Materials and Structures*, (Eds: R. Gilat, L. Banks-Sills), Springer, Dordrecht, The Netherlands **2009**, p. 187.
[93] R. K. Nalla, J. H. Kinney, R. O. Ritchie, *Biomaterials* **2003**, *24*, 3955.
[94] R. O. Ritchie, J. H. Kinney, J. J. Kruzic, R. K. Nalla, *Fatigue Fract. Eng. Mater. Struct.* **2005**, *28*, 345.
[95] M. Petrtyl, J. Hert, P. Fiala, *J. Biomech.* **1996**, *29*, 161.
[96] W. Yang, J. McKittrick, *Acta Biomater.* **2013**, *9*, 9065.
[97] M. A. Meyers, P.-Y. Chen, M. I. Lopez, Y. Seki, A. Y. M. Lin, *J. Mech. Behav. Biomed. Mater.* **2011**, *4*, 626.
[98] Y. Seki, M. S. Schneider, M. A. Meyers, *Acta Mater.* **2005**, *53*, 5281.
[99] H. Rhee, M. F. Horstemeyer, Y. Hwang, H. Lim, H. El Kadiri, W. Trim, *Mater. Sci. Eng. C* **2009**, *29*, 2333.
[100] S. G. Bodde, M. A. Meyers, J. McKittrick, *J. Mech. Behav. Biomed. Mater.* **2011**, *4*, 723.
[101] S. Ravindran, *Sci. Am.* **2013**, *309*, 14.
[102] L. J. Gibson, M. F. Ashby, *Cellular Solids: Structure and Properties*, 2nd ed., Cambridge University Press, Cambridge, UK **1997**.
[103] L. J. Gibson, *J. Biomechanics* **2005**, *38*, 377.
[104] M. F. Ashby, *Metall. Mater. Trans. A* **1983**, *14*, 1755.
[105] Y. Seki, S. G. Bodde, M. A. Meyers, *Acta Biomater.* **2010**, *6*, 331.
[106] Z. Q. Liu, D. Jiao, M. A. Meyers, Z. F. Zhang, *Acta Biomater.* **2015**, *17*, 137.
[107] G. N. Karam, L. J. Gibson, *Int. J. Solids Struct.* **1995**, *32*, 1259.
[108] G. N. Karam, L. J. Gibson, *Int. J. Solids Struct.* **1995**, *32*, 1285.
[109] F. B. Gill, *Ornithology*, 3rd ed., W.H. Freeman & Company, New York **2007**.
[110] N. S. Proctor, P. J. Lynch, *Manual of Ornithology: Avian Structure and Function*,:Yale University Press, New Haven, CT, USA **1993**.
[111] P. M. O'Connor, L. P. A. M. Claessens, *Nature* **2005**, *436*, 253.
[112] J. D. Currey, R. M. Alexander, *J. Zool.* **1985**, *206*, 453.
[113] W. C. Young, R. G. Budynas, A. M. Sadegh, *Roark's Formulas for Stress and Strain*, 8th ed.McGraw Hill, New York **2012**.
[114] C. J. Pennycuick, *Modelling the Flying Bird*, Elseview Academic Press, San Diego, CA, USA **2008**.
[115] I. H. Chen, W. Yang, M. A. Meyers, unpublished.
[116] C. W. Nicolay, M. J. Vaders, *J. Morphol.* **2006**, *267*, 841.
[117] C. R. Jaslow, *J. Biomech.* **1990**, *23*, 313.
[118] J. H. Song, S. Reichert, I. Kallai, D. Gazit, M. Wund, M. C. Boyce, C. Ortiz, *J. Struct. Biol.* **2010**, *171*, 318.
[119] I. C. Gebeshuber, J. H. Kindt, J. B. Thompson, Y. Del Amo, H. Stachelberger, M. A. Brzezinski, G. D. Stucky, D. E. Morse, P. K. Hansma, *J. Microsc.-(Oxford)* **2003**, *212*, 292.
[120] I. H. Chen, J. H. Kiang, V. Correa, M. I. Lopez, P.-Y. Chen, J. McKittrick, M. A. Meyers, *J. Mech. Behav. Biomed. Mater.* **2011**, *4*, 713.
[121] Y. Li, C. Ortiz, M. C. Boyce, *Phys. Rev. E* **2012**, *85*, 031901.
[122] E. Stokstad, *Science* **2005**, *307*, 827.
[123] Y. Li, C. Ortiz, M. C. Boyce, *Phys. Rev. E* **2011**, *84*, 062904.
[124] E. Lin, Y. N. Li, J. C. Weaver, C. Ortiz, M. C. Boyce, *J. Mater. Res.* **2014**, *29*, 1867.
[125] W. Yang, I. H. Chen, B. Gludovatz, E. A. Zimmermann, R. O. Ritchie, M. A. Meyers, *Adv. Mater.* **2013**, *25*, 31.
[126] A. Sosinka, M. M. Rost-Roszkowska, J. Vilimova, K. Tajovsky, M. Kszuk-Jendrysik, L. Chajec, L. Sonakowska, K. Kaminska, M. Hyra, I. Poprawa, *Arthopod Struct. Development* **2014**, *43*, 477.
[127] A. Browning, C. Ortiz, M. C. Boyce, *J. Mech. Behav. Biomed. Mater.* **2013**, *19*, 75.
[128] J. Cornfield, *Sci. Am.* **2008**, *18*, 58.
[129] A. Mitchell, *Nature* **1998**, *391*, 842.
[130] F. J. Vernerey, F. Barthelat, *J. Mech. Phys. Solids* **2014**, *68*, 66.
[131] F. J. Vernerey, F. Barthelat, *Int. J. Solids Struct.* **2010**, *47*, 2268.
[132] F. J. Vernerey, K. Musiket, F. Barthelat, *Int. J. Solids Struct.* **2014**, *51*, 274.
[133] D. J. Zhu, L. Szewciw, F. Vernerey, F. Barthelat, *J. Mech. Behav. Biomed. Mater.* **2013**, *24*, 30.
[134] M. M. Porter, D. Adriaens, R. L. Hatton, M. A. Meyers, J. McKittrick, *Science* **2015**, *349*, aaa6683.
[135] T. Praet, D. Adriaens, S. Van Cauter, B. Masschaele, M. De Beule, B. Verhegghe, *Int. J. Numerical Methods Biomed. Eng.* **2012**, *28*, 1028.
[136] C. Neutens, D. Adriaens, J. Christiaens, B. De Kegel, M. Dierick, R. Boistel, L. Van Hoorebeke, *J. Anat.* **2014**, *224*, 710.
[137] P. Fratzl, *J. R. Soc. Interface* **2007**, *4*, 637.
[138] A. Lazaris, S. Arcidiacono, Y. Huang, J.-F. Zhou, F. Duguay, N. Chretien, E. A. Welsh, J. W. Soares, C. N. Karatzas, *Science* **2002**, *295*, 472.
[139] R. M. Erb, R. Libanori, N. Rothfuchs, A. R. Studart, *Science* **2012**, *335*, 199.
[140] E. Munch, M. E. Launey, D. H. Alsem, E. Saiz, A. P. Tomsia, R. O. Ritchie, *Science* **2008**, *322*, 1516.
[141] A. Tampieri, S. Sprio, A. Ruffini, G. Celotti, I. G. Lesci, N. Roveri, *J. Mater. Chem.* **2009**, *19*, 4973.
[142] B. G. Compton, J. A. Lewis, *Adv. Mater.* **2014**, *26*, 5930.
[143] M. Mirkhalaf, A. K. Dastjerdi, F. Barthelat, *Nat. Commun.* **2014**, *5*, 3166.
[144] X.-X. Xia, Z.-G. Qian, C. S. Ki, Y. H. Park, D. L. Kaplan, S. Y. Lee, *Proc. Natl. Acad. Sci. USA* **2010**, *107*, 14059.
[145] F. Vollrath, D. P. Knight, *Nature* **2001**, *410*, 541.

[146] S. G. Zhang, *Nat. Biotechnol.* **2003**, *21*, 1171.
[147] L. K. Grunenfelder, N. Suksangpanya, C. Salinas, G. Milliron, N. Yaraghi, S. Herrera, K. Evans-Lutterodt, S. R. Nutt, P. Zavattieri, D. Kisailus, *Acta Biomater.* **2014**, *10*, 3997.
[148] G. Milliron, *Ph.D. Thesis*, UC Riverside, Riverside, CA, USA **2012**.
[149] S. Deville, E. Saiz, R. K. Nalla, A. P. Tomsia, *Science* **2006**, *311*, 515.
[150] F. Bouville, E. Maire, S. Meille, B. Van de Moortele, A. J. Stevenson, S. Deville, *Nat. Mater.* **2014**, *13*, 508.
[151] M. M. Porter, M. Yeh, J. Strawson, T. Goehring, S. Lujan, P. Siripasopsotorn, M. A. Meyers, J. McKittrick, *Mater. Sci. Eng. A* **2012**, *556*, 741.
[152] I. Corni, T. J. Harvey, J. A. Wharton, K. R. Stokes, F. C. Walsh, R. J. K. Wood, *Bioinspiration Biomimetics* **2012**, *7*, 031001.
[153] L. Kou, C. Gao, *Nanoscale* **2013**, *5*, 4370.
[154] C. Sachs, H. Fabritius, D. Raabe, *J. Struct. Biol.* **2008**, *161*, 120.

Adv. Mater. **2015**,
DOI: 10.1002/adma.201502403